SAND2015-8604R

SANDIA REPORT

SAND2015-XXXX
Limited Release
Printed September 2015

A Multi-Year Plan for Enhancing Turbulence Modeling in Hydra-TH Revised and Updated Version 2.0

T.M. Smith, M. Berndt, E. Baglietto and B. Magolan

Prepared by
Sandia National Laboratories
Albuquerque, New Mexico 87185 and Livermore, California 94550

Sandia National Laboratories is a multi-program laboratory managed and operated by Sandia Corporation, a wholly owned subsidiary of Lockheed Martin Corporation, for the U.S. Department of Energy's National Nuclear Security Administration under contract DE-AC04-94AL85000.

Issued by Sandia National Laboratories, operated for the United States Department of Energy by Sandia Corporation.

Available to DOE and DOE contractors from
U.S. Department of Energy
Office of Scientific and Technical Information
P.O. Box 62
Oak Ridge, TN 37831

Telephone: (865) 576-8401
Facsimile: (865) 576-5728
E-Mail: reports@adonis.osti.gov
Online ordering: http://www.osti.gov/bridge

Available to the public from
U.S. Department of Commerce
National Technical Information Service
5285 Port Royal Rd
Springfield, VA 22161

Telephone: (800) 553-6847
Facsimile: (703) 605-6900
E-Mail: orders@ntis.fedworld.gov
Online ordering: http://www.ntis.gov/help/ordermethods.asp?loc=7-4-0#online

SAND2015-XXXX
Limited Release
Printed September 2015

A Multi-Year Plan for Enhancing Turbulence Modeling in Hydra-TH Revised and Updated Version 2.0

Thomas M. Smith
Sandia National Laboratories
tmsmith@sandia.gov

Markus Berndt
Los Alamos National Laboratory
berndt@lanl.gov

Emilio Baglietto
Ben Magolan
Massachusetts Institute of Technology
emiliob@mit.edu
benmagolan@gmail.com

Abstract

The purpose of this report is to document a multi-year plan for enhancing turbulence modeling in Hydra-TH for the Consortium for Advanced Simulation of Light Water Reactors (CASL) program. Hydra-TH is being developed to the meet the high-fidelity, high-Reynolds number CFD based thermal hydraulic simulation needs of the program. This work is being conducted within the thermal hydraulics methods (THM) focus area. This report is an extension of THM CASL milestone L3:THM.CFD.P10.02 [33] (March, 2015) and picks up where it left off. It will also serve to meet the requirements of CASL THM level three milestone, L3:THM.CFD.P11.04, scheduled for completion September 30, 2015. The objectives of this plan will be met by: maturation of recently added turbulence models, strategic design/development of new models and systematic and rigorous testing of existing and new models and model extensions. While multi-phase turbulent flow simulations are important to the program, only single-phase modeling will be considered in this report. Large Eddy Simulation (LES) is also an important modeling methodology. However, at least in the first year, the focus is on steady-state Reynolds Averaged Navier-Stokes (RANS) turbulence modeling.

Acknowledgement

The first author is grateful to Russell Hooper for reviewing the report and making valuable suggestions that have led to a more readable report.

1 Executive Summary

The purpose of this report is to document a multi-year plan for enhancing turbulence modeling in Hydra-TH. In Phase II of the Consortium for Advanced Simulation of Light Water Reactors (CASL) program, enhanced turbulence modeling capabilities have been identified as a critical component to high fidelity CFD based thermal hydraulic simulations. Hydra-TH is being developed to the meet the high-fidelity, high-Reynolds number CFD based thermal hydraulic simulation needs of the program. This work is being conducted within the thermal hydraulics methods (THM) focus area. This report is an extension of THM CASL milestone L3:THM.CFD.P10.02 [33] (March, 2015) and picks up where it left off. It will also serve to meet the requirements of CASL THM level three milestone, L3:THM.CFD.P11.04, scheduled for completion September 30, 2015.

The objectives of this plan will be met by: maturation of recently added turbulence models, strategic design/development of new models and systematic and rigorous testing of existing and new models and model extensions. The major objectives include:

1. Mature existing and implement new single-phase turbulence models in Hydra-TH,
2. Plan for the refactor and extendion near wall model treatment,
3. Plan for the extention of models to treat buoyancy driven flows, both thermal and solutal,
4. Address stretch goals: boundary conditions,
5. Address miscellaneous items: limiting ε, user defined inlet profiles, post-processing,
6. Construct turbulence "torture tests" for rigorous testing of individual models and solution verification.

While multi-phase turbulent flow simulations are important to the program, only single-phase modeling will be considered in this report. Large Eddy Simulation (LES) is also an important modeling methodology. However, at least in the first year, the focus is on steady-state Reynolds Averaged Navier-Stokes (RANS) turbulence modeling. Target applications include full reactor core models which will contain tens to hundreds of millions of cells. For these applications, RANS modeling methodology is the only viable alternative and therefore is the focus of the planned work.

The intent is that this document also serve as a conduit for interaction and collaboration within the Hydra-TH development team. This is a multi-year plan and while a large portion of the plan has been completed in this first year, a lot of work still remains and will be reported on in subsequent milestone reports.

The objectives listed above are discussed at length in §2-9, and a summary is given in §10.

2 Overview of Enhanced Turbulence Modeling Plan

The purpose of this document is to organize a plan for enhanced turbulence modeling capabilities in Hydra-TH for the CASL program under the THM focus area. The development plan has two major parts: design/development and rigorous testing - and spans two to three years. This document is a work in progress. It will be periodically updated as new modeling requirements emerge and as test results become available.

Currently, Hydra-TH relies on two production level RANS models; Spalart-Allmaras and RNG $k-\varepsilon$. In the first year, four proposed single-phase RANS turbulence models have been considered for development: standard $k-\varepsilon$, nonlinear $k-\varepsilon$, realizable $k-\varepsilon$ and SST $k-\omega$. The standard model was added after RNG to provide a baseline for all of the various versions of $k-\varepsilon$. In terms of software design, a base class for $k-\varepsilon$ models has been written by B. Magolan with the goal that all variants will inherit from this base class. It has been exercised on several torture test problems and is ready to be promoted to the master branch of the code base. The nonlinear $k-\varepsilon$ has been implemented and exercised on the fuel rod sub-channel secondary flow problem § 9.17, (see Magolan et al. [24]). It has also been exercised on several torture test problems and is ready to be promoted to the master branch of the code base. Finally, the realizable $k-\varepsilon$ model has been implemented and exercised on several torture tests. It is ready to be promoted to the master branch of the code base. The SST $k-\omega$ model is documented in the theory manual but the code completion will occur in the second year.

Planning for near wall treatment and buoyancy closure development will also take place in the first year. At this point in the planning process, near wall treatment encompasses both low-Reynolds number damping functions that allow for integration of the turbulence equations through the boundary layer and wall functions that replace the solution to the governing equations in the cell next to the wall with a solution derived from the law-of-the-wall [23].

In the second year work will begin on near wall treatment and buoyancy closure terms. Hydra-TH has one version of a wall function called the y*-insensitive model [8]. Currently the y*-insensitive wall function is used by the RNG, standard, nonlinear and realizable $k-\varepsilon$ models. The near wall treatment code will be refactored with the goal of encapsulating all modeling terms appearing in all of the governing equations to ensure consistency in the formulation and implementation and to support new near wall treatments such as low-Re damping functions.

Corrections for buoyancy driven flows both thermal and solutal are necessary for post-LOCA accident scenarios where injection of highly borated coolant is to be simulated. This area is still very much a research area. The first year objective is to review the literature and outline a development plan. Formulation and implementation will begin possibly late in FY15 and continue in FY16.

Two sections § 7 and § 8 containing stretch goals and miscellaneous items are also included. It is valuable to list these goals and items to help assess relative importance, but the priority of these items at this time is lower than those discussed in the previous sections.

Also in the first year a collection of turbulence benchmark problems will be constructed.

This is referred to as the turbulence "torture tests". Execution of these tests by the Hydra-TH team will begin in the first year. It includes fundamental flows that have known behavior designed to rigorously test Hydra-TH for high Reynolds number flows and expose strengths and weaknesses of the individual models. The complexity of the tests increases to mimic sub-system flows encountered in reactor cores. Building from very basic to more complex tests will aid the development process.

The development plan is organized as follows. The proposed RANS models are presented in the next section. Because there are so many variations of $k-\varepsilon$, it is important to precisely document the motivation, references and formulation. A summary of the model formulations is presented in the appendix to help in technical discussions pertaining to formulation issues. Next, the near wall treatment refactor requirements are listed, followed by the buoyancy modeling sections. Stretch goal and miscellaneous items sections are then presented. The torture tests are presented in the next section. Each test is listed in its own sub-section. Each test has an objective, resources and task list section. As work is completed, a comment, status and update sub-section will be added.

Two-phase turbulence modeling is very important to the thermal hydraulics capability. However, it will not be included in the scope of this milestone report. Hydra-TH also contains three Large-Eddy Simulation (LES) models: implicit large-eddy simulation (ILES), Smagorinsky and wall adapted large-eddy (WALE). It also contains a hybrid RANS-LES model called detached-eddy simulation (DES) [8]. Several grid-to-rod-fretting (GTRF) studies of rod/spacer grid models using LES have been conducted with Hydra-TH [7] [10]. Several torture test problems such as the Elmahdi 3x3 Rod/Spacer Grid, Impinging Jet and T-Junction discussed in §9 may include LES models along with RANS models for comparison, however, RANS model development is the main focus of this report.

This completes the planning portion of the document. Finally, a brief summary is presented.

3 Implementation of New Turbulence Models

In this section we discuss the proposed modeling development effort which includes maturation of standard and nonlinear $k-\varepsilon$ models and two new models: Realizable $k-\varepsilon$ and SST $k-\omega$. A snapshot of RANS turbulence models is shown in Table 1. A more in depth discussion of the specific formulations can be found in the Hydra-TH theory manual [8] and a brief description of the models can be found in the appendix of this report. It should be mentioned that the theory manual discusses two additional models, namely; $k-\varepsilon-v^2-f$ and $k-\varepsilon-\zeta-f$, however, these two models are not presently included in this development plan.

Model Name	Status	Documented	Regression Tested	Enhancements	Buoyancy	Near Wall Treatment
Spalart-Allmaras	production	Theory Manual	yes	curv. and rot. correction	NA	yes built in
Standard $k-\varepsilon$	ready for promotion	Theory Manual	no	no	Boussinesq	y*-insensitive
RNG $k-\varepsilon$	production	Theory Manual	yes	no	Boussinesq	y*-insensitive
Nonlinear $k-\varepsilon$	ready for promotion	Theory Manual	no	no	Boussinesq	y*-insensitive
Realizable $k-\varepsilon$	ready for promotion	Theory Manual	no	no	Boussinesq	y*-insensitive
SST $k-\omega$	formulation code design	Theory Manual	NA	no	no	NA

Table 1: Summary list of RANS turbulence model development activities in Hydra-TH.

3.1 Mature Standard $k-\varepsilon$ Model

The standard $k-\varepsilon$ model has received less attention in Hydra-TH than the RNG $k-\varepsilon$ model has. It is closely related to the nonlinear $k-\varepsilon$ discussed in § 3.2. It will serve as a baseline with which to judge the nonlinear, realizable and SST$k-\omega$ models discussed in § 3.2, 3.3, 3.4.

Resources:

1. Jones, W.P. and Launder, B.E.,"The Prediction of Laminarization with a Two-Equation Model of Turbulence," International Journal of Mass Transfer, vol. 15, pp. 301–314, 1972.

2. Jones, W.P. and Launder, B.E.,"The Calculation of Low-Reynolds-Number Phenomena with a Two-Equation Model of Turbulence," International Journal of Mass Transfer, vol. 16, pp. 1119–1130, 1973.

3. Launder, B.E.and Spalding, D.B., "The Numerical Computation of Turbulent Flows", Computer Methods in Applied Mechanics and Engineering, vol. 3, pp. 269–289, 1974.

4. Durbin, P.A. and Pettersson Reif, B.A., "Statistical Theory and Modeling for Turbulent Flows, 2nd ed., 2011.

5. Wilcox, D.C., "Turbulence Modeling for CFD," 2nd. ed. 1998.

Tasks:

1. Construct base class for all $k-\varepsilon$ models.
2. Each implementation should derive from base class.
3. Verify that each implementation is correct.
4. Verify by running select turbulence torture tests § 9.
5. Document the model in the theory and user manuals.

Comments and Status:

B. Magolan has constructed a base class from which the standard model derives. At this point the model has been implemented and run on several example problems. It has not been rigorously verified for correctness.

Update

The standard model has been extensively tested on several turbulence torture tests including; grid-turbulence, fully developed pipe flow, impinging jet flow, natural convection, free shear layer and backward facing step. The code resides in a branch of the LANL git repository called "BenKE". The formulation is documented in the Hydra-TH theory manual [8] and usage is documented in the Hydra-TH user manual [9]. Remaining tasks include: promotion to the master branch and addition of regression tests.

3.2 Mature Nonlinear $k-\varepsilon$ Model

There are two main differences between the nonlinear $k-\varepsilon$ and the standard $k-\varepsilon$ model. The first is that instead of a constant C_μ, it is considered a function of the mean stress which is meant to improve robustness by satisfying realizability constraints on the Reynolds stresses. The second is that the Reynolds stresses are assumed to have a quadratic and possibly cubic dependence on mean stresses. It has been argued by Baglietto and Nanokata (see resources below) that the nonlinear dependence is necessary to capture secondary flows in sub-channels.

Resources:

1. Baglietto and Nanokata, "Improved Turbulence Modeling for Performance Evaluation of Novel Fuel Designs," Nuclear Technology vol. 158, 2006.
2. Baglietto, E., "Anisotropic Turbulence Modeling of Accurate Rod Bundle Simulations," ICONE 14, 2006.
3. Magolan, B. et al., "Non-Linear Eddy Viscosity Turbulence Modeling in Hydra-TH for Fuel Related Applications," NURETH-16, 2015.

Tasks:

1. Implementation should derive from base class.
2. Verify that the implementation of the model and linearization terms are correct.
3. Verify by running the sub-channel torture test problem § 9.17.
4. Couple to low-Re damping functions
5. Document the model in the theory and user manuals.

Comments and Status:

This model has been implemented and tested extensively on the sub-channel secondary flow problem (see §9.17). Some maturation of the implementation and implicit terms remains.

Update

Magolan has completed the implementation and validated the model on the sub-channel torture test. It has also been exercised on grid-turbulence, Couette flow and impinging jet flow. The code resides in a branch of the LANL git repository called "BenKE". The formulation is documented in the Hydra-TH theory manual [8] and usage is documented in the Hydra-TH user manual [9]. Remaining tasks include: promotion to the master branch and addition of regression tests.

3.3 Realizable $k-\varepsilon$ Model

The realizable $k-\varepsilon$ model differs from the standard model in two main respects;

- C_μ is no longer constant, it is a function of the mean strain S_{ij} so that the Reynolds stresses remain realizable (i.e., The Schwartz inequality for the Reynolds stresses is satisfied), and
- a new dissipation rate equation is derived based on the transport equation of mean-square vorticity fluctuation.

Resources:

1. Shih et al., "A Realizable Reynolds Stress Algebraic Equation Model," NACA-TM-105993, 1993.
2. Shih et al., "A New Reynolds Stress Algebraic Equation Model," NACA-TM-106644, 1994.
3. Shih et al., "A New $k-\varepsilon$ Eddy Viscosity Model for High Reynolds Number Turbulent Flows," Computers and Fluids, 1995.

Tasks:

1. Choose the formulation.
2. Prepare a design document and vet with Hydra-TH team.
3. Implement the design.
4. Verify the model is implemented correctly.
5. Couple to wall function.
6. Document in theory and user manuals.

Comments and Status:

The formulation based strictly on the references listed above has been chosen.

Update

This model has been implemented and tested on the grid-turbulence torture test §9.3 and mixing layer flows §9.5. The code resides in a local branch called "tmsmithRKE" (contact T.M. Smith). The formulation is documented in the Hydra-TH theory manual [8] and usage is documented in the Hydra-TH user manual [9]. Remaining tasks include: promotion to the master branch and addition of regression tests.

3.4 SST $k-\omega$ Model

Menter's shear stress transport (SST) $k-\omega$ model [25] blends Wilcox's $k-\omega$ model [38] with the standard $k-\varepsilon$ model where the ε equation, representing the rate of turbulent kinetic energy dissipation, is rewritten as an equation for ω, which approximately represents the time scale for energy dissipation. Units for ε are (ℓ^2/t^3) and for ω are $(1/t)$. Several motivations for choosing this model over the standard $k-\varepsilon$ or the $k-\omega$ model include:

- The $k-\omega$ model and SST version do not require the use of special near wall treatments and can be integrated to the wall directly.
- SST $k-\omega$ eliminates the sensitivity to free stream in ω that hampers the Wilcox $k-\omega$ model.
- SST $k-\omega$ incorporates transport of Reynolds stress (as the name implies) which results in better predictions in flows with strong pressure gradients.

Resources:

1. Menter, "Two-Equation Eddy-Viscosity Turbulence Models for Engineering Applications," AIAA Journal, vol. 32, 1994.

2. Menter, "Improved Two-Equation $k-\omega$ Turbulence Models for Aerodynamic Flows," NASA TM-103975, 1992.

3. Also see Hydra-TH Theory Manual [8].

Tasks:

1. Choose the formulation.

2. Prepare a design document and vet with Hydra-TH team.

3. Implement the design.

4. Verify the model is implemented correctly.

5. Document in theory and user manuals.

Comments and Status:

The formulation is documented in the Hydra-TH theory manual [8] and a skeleton of model has been coded.

4 Refactor Near Wall Model Treatment

Objectives:

1. Achieve complete coverage on all $k-\varepsilon$ models.
2. Refactor to a more flexible software design that supports multiple wall functions and low-Re damping functions.
3. Strive for "plug and play" interoperable functionality.
4. To extent possible, implement in virtual base classes.

Resources:

1. There are references available in the Hydra-TH repository, https://hydra.lanl.gov/redmine/projects/casl-documentation/repository/references/revisions/master/show/topics/turbulence/Wall-Turbulence.
2. Hydra-TH has an implementation of the y*-insensitive wall function that is active when the STD, RNG, NL or RKE $k-\varepsilon$ models are used.
3. There is a description of the formulation and implementation of the y*-insensitive wall function in the Hydra-TH theory manual [8]. Four low-Reynolds number damping function formulations are also presented in Appendix B.
4. Launder, B.E. and Spalding, D.B., "The Numerical Computation of Turbulent Flows," Computer Methods in Applied Mechanics and Engineering, vol. 3, pp. 269–289, 1974.
5. Defraeye, T., Blocken, B. and Carmeliet, J., "CFD analysis of convective heat transfer at the surfaces of a cube immersed in a turbulent boundary layer", International Journal of Heat and Mass Transfer, vol. 53, no. 1, pp. 297–308, 2010.
6. Hanjalic, K. and Launder, B., "Modelling Turbulence in Engineering, Second-Moment Routes to Closure", Cambridge University Press, 2011.
7. Wilcox, D.C., "Turbulence Modeling for CFD," 2nd. ed., pp. 187-188, 1998.
8. Lam, C.K.G. and Bremhorst, K., "A Modified Form of the $k-\varepsilon$ Model for Predicting Wall Turbulence," Journal of Fluids Engineering, vol. 103, pp. 456–460, 1981.
9. Davidson, L., "Calculation of the Turbulent Buoyancy-Driven Flow in a Rectangular Cavity Using an Efficient Solver and Two Different Low Reynolds Number $k-\varepsilon$ Turbulence Models," Numerical Heat Transfer, Part A, vol. 18, pp. 129–147, 1990.
10. Patel, V.C., Rodi, W. and Scheuerer, G., "Turbulence Models for Near-Wall and Low Reynolds Number Flows: A Review," AIAA Journal, vol. 123, no. 9, pp. 1308–1319, 1985.
11. Albets-Chico, X., Perez-Segarra, C.D., Oliva, A. and Bredberg, J., "Analysis of wall-function approaches using two-equation turbulence models," International Journal of Heat and Mass Transfer, vol. 51, pp. 4940–4957, 2008.

Tasks:

1. Ensure wall functions are operational for all $k-\varepsilon$ models.
2. Literature search.
3. Gather requirements.
4. Define wall function formulations.
5. Define low-Re formulations.
6. Ensure consistency between wall model surface output delegates.
7. Verify that the implementations are correct.
8. Document models in the theory and user manuals.
9. Verify by running turbulence torture tests § 9.

Comments and Status:

All variations of $k-\varepsilon$ models require some form of near wall treatment for wall bounded flows. There is a large class of problems in CASL where the quantities of interest from Hydra-TH simulations will depend on accurate surface data such as: wall temperature, heat flux and shear stress. Complex geometry and highly swirling flow patterns cause variations in y^+ which complicate the task of generating "optimal" meshes for the accurate wall model behavior. The y*-insensitive model outlined in Grotjans and Menter [18] is designed to handle this variable y^+ issue. This issue will have to be addressed when considering new formulations of wall models and low-Re damping functions for implementation in Hydra-TH. Additionally, it will be a challenge to ensure accurate surface output data from simulations using wall functions or low-Re damping functions.

The law-of-the-wall which has been observed by Coles [11] describes the mean velocity profile in terms of a viscous sublayer, buffer layer, logarithmic layer and outer layer. In the viscous sublayer, viscous damping and near wall proximity dominate, and the role of turbulence fluctuations is diminished as the wall is approached. In this layer $y^+ \approx U^+$ where $y^+ = \rho u_\tau y/\mu$ and the friction velocity is $u_\tau = \sqrt{\frac{\tau_w}{\rho}}$. In the logarithmic region (inertial layer) turbulent fluctuations dominate and the mean velocity follows $U^+ \equiv \frac{1}{\kappa}\ln Ey^+$. The buffer region which is not distinct is the overlap region between the viscous sublayer and the inertial layer. In the outer layer intermittency plays an important role, but is of less concern in near wall modeling.

Similarly, assuming Reynolds analogy, a non-dimensional temperature at y_p can be derived

$$T^+ \equiv \frac{(T_w - T)\,\rho C_p u_\tau}{\dot{q}''_w} = Prt\left[\frac{1}{\kappa}\ln Ey^+ + P_J\right] \tag{1}$$

which provides a way to compute the heat flux given the wall temperature and to compute wall temperature given wall heat flux.

The basic idea of the y*-insensitive wall function is to specify the normal wall distance in the cell adjacent to the wall such that the integration point y_p lies above the point where the viscous sublayer and the inertial layer intersect $y_v \approx 11.225$. The production and dissipation source terms in the k-equation are replaced with formulas derived from the law-of-the-wall, and the ε-equation is discarded in this first cell and its value is determined by the law-of-the-wall. In addition, effective viscosity and conductivity coefficients are determined from the law-of-the-wall.

New velocity and length scales y^* and U^* are adopted replacing y^+ and U^+. The reason is that it has long been understood that for stagnation flows such as an impinging jet on a flat plate and recirculating flow such as the region upstream of reattachment in a backward facing step flow, the wall shear τ_w goes to zero and so y^+ is undefined. The new scales, y^* and U^* are based on turbulent kinetic energy

$$y^* = \frac{\rho C_\mu^{1/4} y k^{1/2}}{\mu} \qquad U^* = \frac{\rho C_\mu^{1/4} u k^{1/2}}{\tau_w}$$

and under conditions of equilibrium, production equals dissipation, and

$$\sqrt{\frac{\tau_w}{\rho}} = C_\mu^{1/4} k^{1/2}.$$

The y*-insensitive model assumes a two-layer representation of the near wall boundary layer and adjusts the location of the integration point in the cell adjacent to the wall if it is located in the viscous sublayer $y^*_{p,lim} = \max(y^*_p, y^*_v)$. The new location for the integration point is $y_{p,lim} = \frac{y^*_{p,lim}\mu}{\rho C_\mu^{1/4} k^{1/2}}$. The turbulent kinetic energy production is

$$P_k = \begin{cases} 0 & y^*_p < y^*_v \\ \frac{\tau_w^2}{\kappa \rho C_\mu^{1/4} k^{3/2} y_p} & y^*_p > y^*_v. \end{cases}$$

The wall shear is now determined from k and y^* instead of u_τ and is given by

$$\tau_w = \frac{C_\mu^{1/4} \rho u_p k^{1/2}}{\frac{1}{\kappa}\ln(E y^*_p)}. \tag{2}$$

The dissipation equation is replaced in the first adjacent cell with

$$\varepsilon = \begin{cases} \frac{2\mu k}{y_v^2} & y^*_p < y^*_v \\ \frac{\rho C_\mu^{3/4} k^{3/2}}{\kappa y_p} & y^*_p > y^*_v. \end{cases}$$

In the relatively large wall adjacent cells, production and dissipation can vary significantly with wall normal spacing so an average value is obtained by integrating in the wall normal direction

$$\begin{aligned} P_{k,ave} &= \frac{1}{y_n}\int_0^{y_n} P_k dy = \frac{\tau_w^2}{\rho\kappa C_m u^{1/4} k^{1/2} y_n \ln\left(\frac{y_n}{y_v}\right)} \\ D_{k,ave} &= \frac{1}{y_n}\int_0^{y_n} D_k dy = \frac{2\mu k}{y_n y_v} + \frac{\rho C_m u^{3/4} k^{3/2}}{\kappa y_n}\ln\left(\frac{y_n}{y_v}\right). \end{aligned}$$

In addition to modifying the production and dissipation source terms in the k-equation, and specifying the ε, momentum and energy transport coefficients are modified

$$\mu_{eff} = \begin{cases} \mu & y_p^* < y_v^* \\ \frac{\rho C_\mu^{1/4} k^{1/2} y_p}{\frac{1}{\kappa}\ln\left(E y_p^*\right)} & y_p^* > y_v^* \end{cases} \tag{3}$$

$$\kappa_{eff} = \frac{\mu C_p y_p^*}{T^*} \tag{4}$$

where

$$T^* = \begin{cases} Pr y_p^* & y_p^* < y_v^* \\ Prt\left(\frac{1}{\kappa}\ln(E y_p^*) + P_J\right) & y_p^* > y_T^* \end{cases}$$

where y_T^* depends on the molecular and turbulent Prandtl numbers. From this formulation emerges a way to estimate the wall temperature given the wall heat flux and compute the wall heat flux given the wall temperature

$$\dot{q}_w'' = \frac{\left[T_w - T_p\right]\rho C_p C_\mu^{1/4} k^{1/2}}{Prt\left(\frac{1}{\kappa}\ln(E y_p^*) + P_J\right)} \tag{5}$$

where P_J is the Jayatilleke (1969) function

$$P_J = 9.0\left[\left(\frac{Pr}{Prt}\right)^{3/4} - 1\right]\left[1 + 0.28\exp\left(-0.007\left(\frac{Pr}{Prt}\right)\right)\right]. \tag{6}$$

P_J provides a measure of the relative resistances to heat and momentum exchange in the sublayer. This completes the description of the y*-insensitive wall function. In addition to using wall functions to derive surface quantities, in the case of specified heat flux boundary condition, the wall temperature is determined from

$$T_w = T_p \frac{\dot{q}_w''}{\kappa_{eff}}(y_p - y_w) \tag{7}$$

where κ_{eff} depends on the turbulence model (e.g., for SA, κ_{eff} is the molecular value).

There has been many attempts to extend the basic model. The book by Hanjalic and Launder [19] and papers by Craft and co-workers [12, 13] give examples of how the model can be extended and enhanced.

Low Reynolds number $k-\varepsilon$ models solve both k and ε equations to the wall such that the wall adjacent cell has a $y^+ \approx 1$ and add damping functions to the equations in order to recover the correct behavior in the near wall region. Patel et al. [28] and Wilcox [39] have reviewed popular versions of these models. The Hydra-TH Theory Manual also lists several of the more popular models.

Based upon predictions of wall shear and Nusselt number in fully developed turbulent pipe flow and impinging jet flow, it is recommended that low-Re models be implemented in Hydra-TH for all $k-\varepsilon$ models.

5 Model Extensions for Buoyancy Driven Thermal and Solutal Flows

Objectives:

1. Research what is the right thing to do, open ended, research (next year).
2. Obtain references from J. Bakosi - in Hydra-TH repository, references directory topics, buoyancy driven flows.
3. Add capability in preparation for the post LOCA injection of highly borated coolant simulations (A. Stagg and S.J. Yoon).
4. Correction to the k-equation production term for buoyancy with large density variations.
5. Achieve complete coverage on all RANS turbulence models.

Resources:

1. Some references are available in the Hydra-TH repository; https://hydra.lanl.gov/redmine/projects/casl-documentation/repository/references/revisions/master/show/topics/turbulence/Buoyancy-driven.
2. Davidson, L., "Second-order Corrections of the $k-\varepsilon$ Model to Account for Non-isotropic Effects Due to Buoyancy," International Journal for Heat and Mass Transfer, vol. 133, no. 12, pp. 2599–2608, 1990.
3. Hydra-TH has implemented a Boussinesq buoyancy body force in the momentum equation and a modification to the turbulent kinetic energy in the STD, RNG, NL and RKE $k-\varepsilon$ models.

Tasks:

1. Choose formulations.
2. Design code implementation.
3. Implement code design.
4. Construct and execute appropriate tests to evaluate new capabilities.
5. Document in user and theory manuals.

Comments and Status:

A baseline for modeling buoyancy driven turbulence in the context of the standard $k-\varepsilon$ model is presented in §11.2. This is based on the work of Davidson [17] and should be considered the launch point for future research and development.

Update:

A baseline assessment of the buoyancy closures in the momentum and k equation has been made by solving a square-cavity natural convection problem (see § 9.16).

6 Two-Phase Turbulence Models

Two-phase flow modeling and two-phase turbulent flow modeling are high priority capabilities for CASL THM. However, two-phase flow turbulence modeling is outside the scope of this report. As of FY2015, the plan is to follow closely the work by Layhe for turbulence closure. Only a partial citation list will be presented below.

Resources:

1. M. Lopez de Bertodano, R. T. Lahey, O. C. Jones, "Development of a k- Model for Bubbly Two-Phase Flow," J. Fluids Eng. 116(1), pp. 128-134, 1994.

2. M. Lopez de Bertodano, S.-J. Lee, R. T. Lahey, D. A. Drew, "The Prediction of Two-Phase Turbulence and Phase Distribution Phenomena Using a Reynolds Stress Model," J. Fluids Eng. 112(1), pp. 107-113, 1990.

3. G.S. Arnold, D.A. Drew, and R.T. Lahey, "Derivation of Constitutive Equations for Interfacial Forces and Reynolds Stress for a Suspension of Spheres Using Ensemble Averaging," Chem. Eng. Communications, vol. 86, pp. 43-54, 1988.

4. Antal, S., Kurul, N., Podowski, M. And Lahey, R.T., Jr., "The Development of Multidimensional Modeling Capabilities for Annular Flows, Proceedings of the International Conference on Multiphase Flow (ICMF), Lyon, France, June 8-12, 1998.

5. Lahey, R.T., Jr., A CFD Analysis of Multidimensional Two-Phase Flow and Heat Transfer Using a Four Field, Two-Fluid Model, Proceedings of the Thirteenth U.S. National Congress on Applied Mechanics, University of Florida, June 21-26, 1998.

7 Stretch Goals

Stretch goals are included in the planning because of the potential impact on turbulence modeling capability, however, the priority may be lower than development goals discussed above.

7.1 Periodic Boundary Conditions

Objectives:

1. Achieve Cartesian axis aligned periodic boundary conditions.

Resources:

1. Look at partial implementation.

Tasks:

1. Complete implementation.

Comments and Status:

Some preliminary work in Hydra-TH has been done.

7.2 General Symmetry Boundary Conditions

Objectives:

1. Implement general (non-Cartesian axis aligned) symmetry (tensor reflection) boundary conditions.

Resources:

1. E. Baglietto is familiar with the formulation and should be consulted.

Tasks:

1. Derive symmetry conditions for arbitrarily oriented face.
2. Produce a design document.
3. Implement in Hydra-TH.

Comments and Status:

The current symmetry boundary conditions are enforced through no-penetration for velocity and no flux specification for scalars. This limits the use of symmetry boundary conditions to axis aligned boundaries. The user would like to be able to specify a symmetry boundary condition on an arbitrarily oriented boundary surface.

8 Miscellaneous Items

8.1 Limiting ε

Objectives:

1. Limit ε in $k-\varepsilon$ models for improving robustness.
2. Determine the best choice for limiting ε.

Resources:

1. Time scaling arguments for stagnating flows (see code).
2. Implementation in Hydra-TH.
3. The current implementation is presented in the Hydra-TH theory manual [8].

Tasks:

1. Do a literature search to determine what information is available.
2. Choose the appropriate tests that express the effects of limiting.
3. Determine how limiting affects robustness.
4. Evaluate time scaling arguments in test flow problems.
5. To extent possible, implement in base class.

Comments and Status:

"On the k-e models, one thing Im wondering about is a bit of probing/research on the setting the lower-bounds for epsilon. I had used a time-scale limiter similar to whats done in k-w and that the guys at Flow Sciences advocate. However, it really only works for stagnation flow. I have some scaling arguments for the lower-bound on dissipation rate and use that for setting a minimum on epsilon, but this could be an interesting and really useful small side-study to understand what is really the best choice." (M.A. Christon, 2-6-15)

Currently, all variations of $k-\varepsilon$ models use the same limiting procedure for ε. The limiters are designed to prevent ε from going below a threshold based on k and a measure of strain rate, $\sqrt{\tilde{S}_{ij}\tilde{S}_{ij}}$

$$\varepsilon_{lim} = \frac{C_{2\varepsilon lim} C_\mu^2}{C_{1\varepsilon lim}} \sqrt{\tilde{S}_{ij}\tilde{S}_{ij}}\ k.$$

The limiter coefficients are $C_{1\varepsilon lim} = 0.85$ and $C_{2\varepsilon lim} = 1.22$ respectively.

8.2 Inflow Boundary Conditions

Objectives:

1. Produce a small number of generally applicable boundary conditions for specifying inflow turbulent profiles.
2. Parabolic and power law 2D and 3D channel profiles.
3. Parabolic and power law 3D pipe.
4. Specify scalars such as temperature and species.
5. Interpolate from data file.

Resources:

1. Hydra-TH does have a mechanism for specifying user defined Dirichlet BCs.

Tasks:

1. Implement user-specified, pre-programmed parabolic and power law distribution profiles for 2D and 3D geometries.
2. Add additional user defined functionality for other dependent variables such as scalars.
3. Implement an interface to read and interpolate boundary data.
4. Add the capability to specify turbulence model variable input profiles.

Comments and Status:

An example of a fully developed turbulent channel flow velocity profile using a 1/7 power law is given by the function

$$U(y) = U_{in}\left(1 - 2\frac{|y - y_c|}{H}\right)^{1/7} \quad y_{\min} \leq y_c \leq y_{\max} \quad H = y_{max} - y_{min} \tag{8}$$

where y_c is the value of the center of the channel and H is the channel width. This produces a symmetric profile about the channel center line with a 1/7 power dependence on the y coordinate. The reference velocity in this case is the value averaged across the channel which can be analytically determined by integrating the profile function. Its value is $0.875\ U_{in}$. This function serves as an example and could easily be modified to produce a parabolic profile for laminar inflow or an arbitrary power law.

There has been some recent work on user defined boundary conditions. It may be possible to exploit this work for the purposes of defining turbulent inflow conditions.

8.3 Post-Processing data

Objectives:

1. Joining distributed Exodus II files into a single plot file for post-processing.
2. Provide an Exodus II based post-processing utility for extracting data from small to medium sized models for the purpose of analysis.

Resources:

1. Schoff, L.A. and Yarberry, V.R., "Exodus II: A Finite Element Data Model Sandia Report," 1994.

Tasks:

1. Write global element number and node number maps to distributed files.
2. Gather additional feature requests for post-processing.
3. Prune un-necessary features.
4. Enrich element library by adding Pyramid5 and Wedge6 elements.
5. Add error handling.
6. Copyright the code?
7. Stretch Goal: Write a version that will process distributed files.

Comments and Status:

An initial code has been written and is currently being exercised. Some development effort remains. The post-processing code only depends on Exodus and Netcdf. It is therefore easily built with versions distributed with Hydra-TH. The code can be executed in a menu driven mode or in a batch driven mode. The code can be obtained from T.M. Smith. Most of the results presented in this report were generated using this new post-processing tool.

Update

The code now includes surface integration for all four three-dimensional element topologies. New functionality has been added that applies wall functions to the solution data to calculate surface quantities more accurately and to aid in the development of wall functions in Hydra-TH for flow solutions and surface delegates for solution output. Volume quadrature for Wedge6 and Pyramid5 element types remains a task for the future.

9 Turbulence Torture Tests

The turbulence torture tests described in this section are intended to provide an archive for solution verification to diverse turbulent flows that may be encountered in nuclear reactors and validation of the turbulence modeling capabilities in Hydra-TH. As this suite of tests matures, it should facilitate rapid prototyping, solution verification and validation of future enhancements by providing information pertaining to problem setup, references, post-processing, Hydra-TH control files and mesh files.

A similar effort was undertaken by Pannala and Stagg [27] in 2012 to define THM CFD benchmark problems. The present effort incorporates several of these benchmark problems into torture test problems.

Candidate problems under consideration are listed in Table 2. Additional candidate problems will be considered based on relevancy and how well the test aligns with the requirements of THM. From the table, the objective column gives a brief description of an expected physical outcome of the solution. The mesh file column refers to whether mesh files exist. Many of these tests only require relatively simple meshes, however, several tests will require sophisticated meshes. Having multiple mesh files with varying resolution available and obtaining solutions on these meshes is necessary for establishing evidence of grid convergence, a necessary but not sufficient metric for determining the quality of the over-all solution.

Problem statements, mesh files, control files and possibly post-processing files will be archived in a separate directory within the Hydra-TH repository. Several tests have been exercised and are in varying states of completeness and are presented in the following sections.

Each test problem is presented below in its own section that describes the test, objectives, resources available, tasks, status and general comments.

Test Name	Dimensions	Objectives	Mesh Files	Status	Documented	Regression Testing
Back Step	2D	Reattachment location	Cubit available	SA, STD	no	yes
Channel	2D	Law-of-the-wall	Cubit available	SA, RNG	Verification Manual	yes
Grid Turbulence	1D	Analytical Solution $k-\varepsilon$	three levels available	RNG, STD, NL, RKE	Verification Manual	yes
Couette Flow	2D	Mean velocity profile	Cubit available	SA, RNG, STD, NL	some	no
Mixing Layer	2D	spreading rate scale similarity	Cubit available	SA, RNG, STD, RKE	some	no
Jets	2D-3D	spreading rate scale similarity	none	not started	no	no
Pipe Flow	3D	Law-of-the-wall Nusselt No.	Cubit available	SA, RNG, STD	some	no
U-Channel	2D	curvature and rotation correction	Cubit available	SA, RNG, STD	some L3 milestone	no
Circular Cylinder	2D	Strouhal No.	Cubit available	SA, RNG	no	yes
Triangular Cylinder	2D	Strouhal No.	no	not started	no	no
Square Cylinder	2D	Strouhal No.	no	not started	no	no
Asymmetric Diffuser	2D	pressure induced separation	no	not started	no	no
Impinging Jet	3D	Stagnation point flow	Cubit available	extensive SA STD, RNG, NL	no	no
Jet in Crossflow	2D	complex vortical structures	no	not started	no	no
Mounted Cube	3D	Massive separation	no	not started	no	no
Square Cavity	3D	Nusselt Number Velocity Profiles	Cubit available	SA, STD	no	no
Sub-Channel Secondary Flow	3D	Secondary flow orientation	Cubit available	extensive NL, STD	presentations NURETH-16	no
3x3 Rod/Spacer	3D	pressure drop	Cubit avail., Hexpress	extensive RNG SA, STD, ILES	Verification Manual	no
T-Junction	3D	Velocity profiles, pressure drop	at least one available	Preliminary ILES	some	no

Table 2: Summary list of turbulence torture tests for Hydra-TH.

9.1 Backward-Facing Step

Objectives:

1. Compute re-attachment point with different models.
2. Compare solutions from different models.

Resources:

1. H. Le, P. Moin and J. Kim, "Direct numerical simulation of turbulent flow over a backward-facing step," J. Fluid Mech. 1997.
2. B. Basara. S. Jarkirlic "A new hybrid turbulence modeling strategy for industrial CFD," IJNMF, 2003.
3. Thakur et al., "Development of Pressure-Based Composite Multigrid Methods for Complex Fluid Flows," Prog. Aerospace Sci., 1996.
4. P. A. Durbin, "Separated Flow Computations with the k-e-v2 Model," AIAA J., 1995.
5. C.G. Speziale, "Analysis of an RNG Based Turbulence Model for Separated Flows," Int J. Eng. Sci., 1992.
6. Ravikanth V.R. Avancha, Richard H. Pletcher, "Large eddy simulation of the turbulent flow past a backward-facing step with heat transfer and property variations," Int. J. of Heat and Fluid Flow, 2002.
7. Albets-Chico, X., Perez-Segarra, C.D., Oliva, A. and Bredberg, J., " Analysis of wall-function approaches using two-equation turbulence models," International Journal of Heat and Mass Transfer, vol. 51, pp. 4940–4957, 2008.
8. Cubit parametrized journal files and meshes available (contact T.M. Smith).

Tasks:

1. Generate meshes.
2. Setup control files and run.
3. Document post-processing.
4. Run different models.

Comments and Status:

An example of this flow is included in the regression test suite. Both SA and RNG $k-\varepsilon$ models are tested. These tests are the starting point for more detailed studies.

Update:

Simulations exercising the SA and STD models have been performed. Analysis of the solutions remains to be done.

9.2 Channel Flow

Objectives:

1. Verify that the different models reproduce law-of-the-wall (y^+ vs. U^+).

Resources:

1. Moser, R.D., Kim, J. and Mansour, N.N., "Direct numerical simulation of turbulent channel flow up to $Re_\tau = 590$", Physics of Fluids, 1999.
2. See Hydra-TH V&V manual [10].
3. Cubit Aprepro parametrized journal files and meshes available (contact T.M. Smith).

Tasks:

1. Reproduce runs presented in the V&V manual for different models.
2. Run different models.

Comments and Status:

An example of this flow is included in the verification test suite. Both SA and RNG $k-\varepsilon$ models are run. From this work, it will be straight forward to run additional studies with different models.

9.3 Grid Turbulence

Objectives:

1. Exercise advection, diffusion, production, dissipation away from walls.
2. Make direct comparisons with analytical solution.

Resources:

1. See Hydra-TH V&V manual [10].
2. Three mesh files and control files for semi-implicit and fully-implicit solution strategies are available in the verification repository.
3. Mohammadi, B. and Pironneau, O., "Analysis of the K-Epsilon Turbulence Model," Wiley New York, 1993.

Tasks:

1. Reproduce runs presented in the V&V manual for new models.

Comments and Status:

Decaying isotropic turbulence in a uniform flow has the following analytic solutions for k and ε,

$$
\begin{aligned}
k(x) &= k_0 \left(1 + (C_2 - 1)x\frac{\varepsilon_0}{k_0 U_0}\right)^{\frac{1}{1-C_2}} \\
\varepsilon(x) &= \varepsilon_0 \left(1 + (C_2 - 1)x\frac{\varepsilon_0}{k_0 U_0}\right)^{\frac{C_2}{1-C_2}} .
\end{aligned}
$$

where C_2 is a constant that depends on the model; STD (1.92), RNG(1.68), NL (1.92) and RKE (1.9). The analytic solutions for RNG are given in the Hydra-TH Verification manual. In the manual U_0 was omitted in eq. 2.57, however, since $U_0 = 1$ the reported solutions are correct. An example of this flow is also included as a regression test suite for the RNG $k - \varepsilon$ model.

Update:

Both semi-implicit and fully-implicit solutions are presented for STD, NL and RKE models. This test runs very quickly and quantities of interest are easy to extract from solution data. The domain is 1x0.1x0.001, density $\rho = 1$ and viscosity $\mu = 1.5e - 6$. Three uniform grids are used; 50x5x1, 100x10x1, 200x20x1 (see Figure 1). Figures 2, 3 and 4 compare the numerical solutions to the analytical solutions and the agreement is very good. While this is not a rigorous verification, results for different mesh resolutions can not be distinguished.

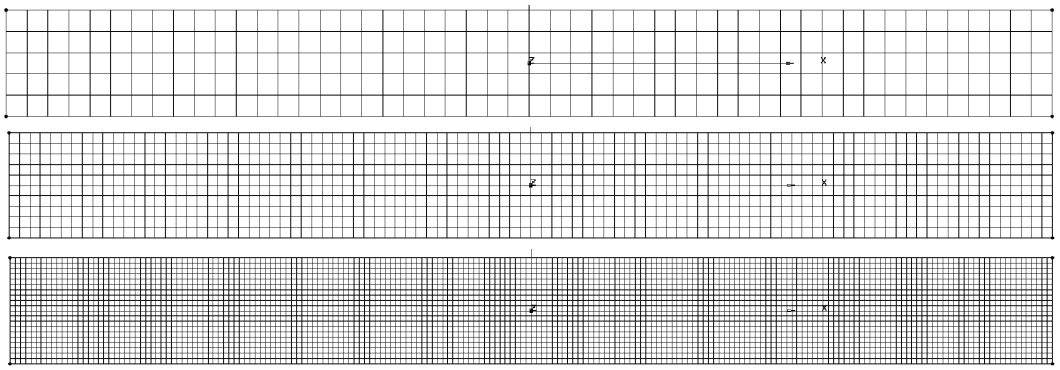

Figure 1: Computational meshes for decaying Grid turbulence,50x5x1,100x10x1,200x20x1.

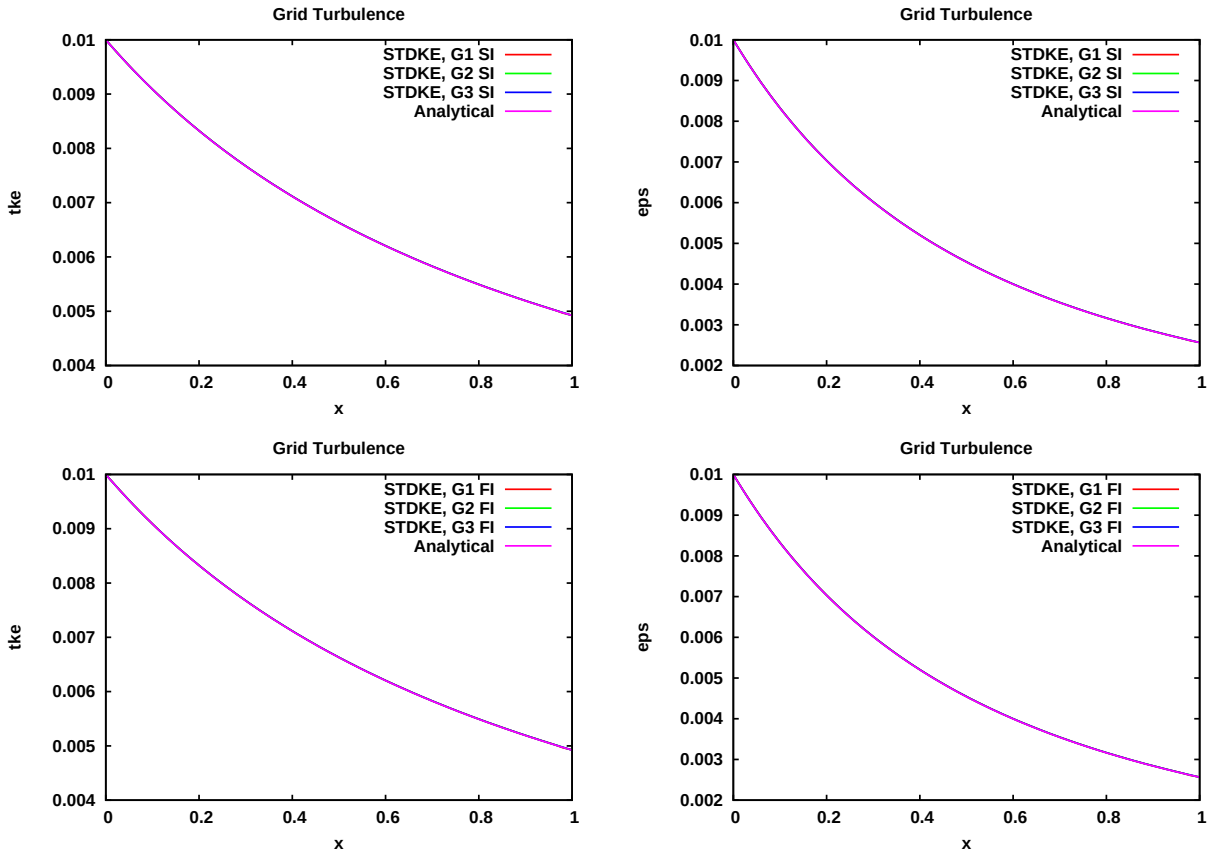

Figure 2: Decaying Grid turbulence - STD model.

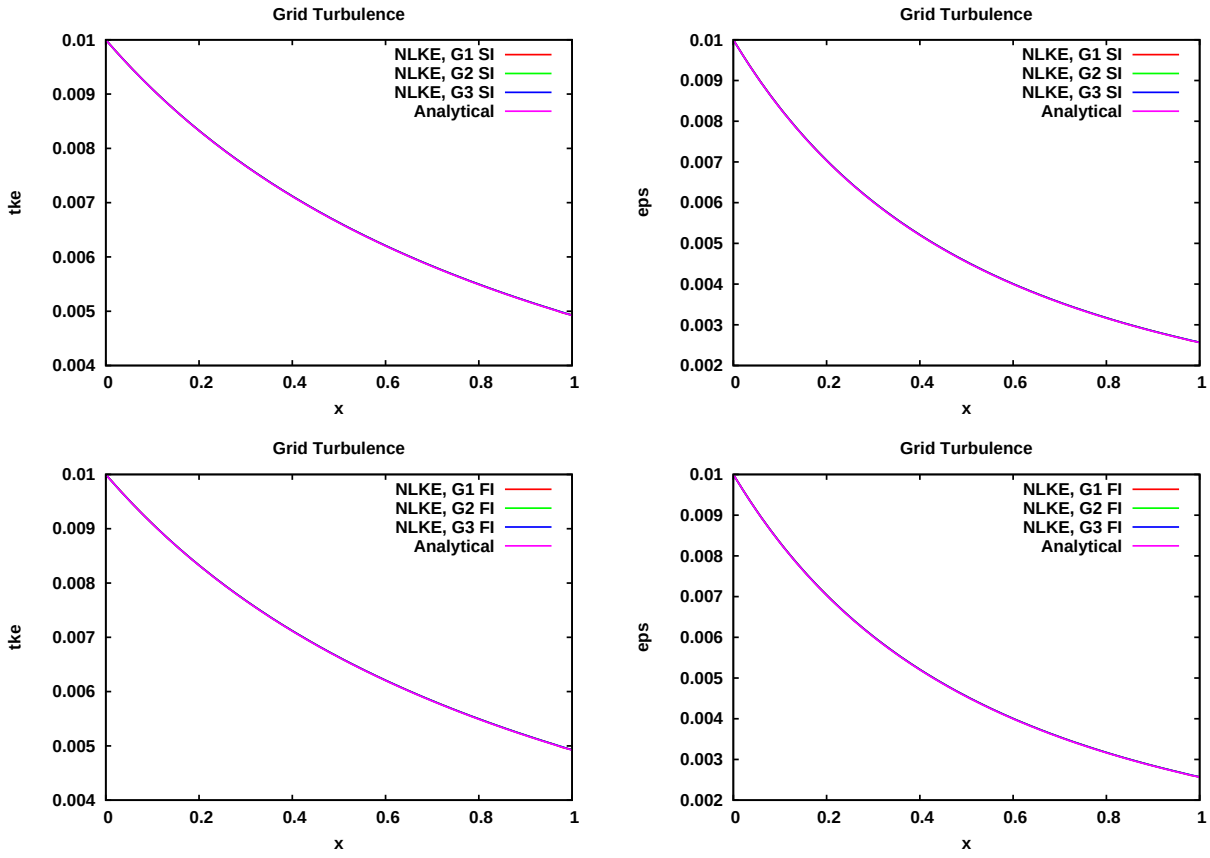

Figure 3: Decaying Grid turbulence - NL model.

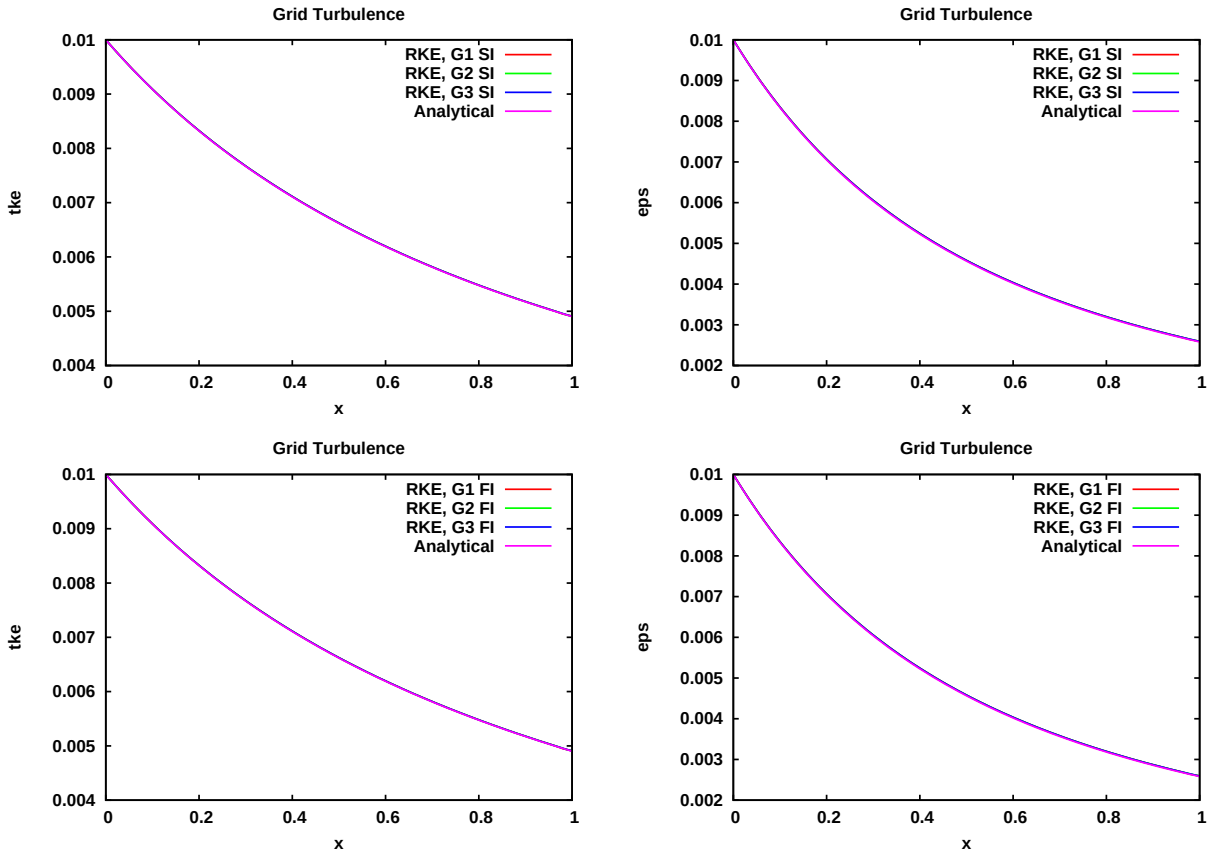

Figure 4: Decaying Grid turbulence - RKE model.

9.4 Couette Flow

Objectives:

1. Verify that the different models reproduce mean velocity profile compared with experimental data.
2. Check for anti-symmetry in vertical profiles.
3. Test near wall treatments of the various RANS models.
4. Compare directly with experimental data.

Resources:

1. Kim, W.-W. and Menon, S., "Application of the localized dynamic subgrid-scale model to turbulent wall-bounded flows," AIAA Paper 97-0210, Jan. 6-9, 1997.
2. Aydin, E.M. and Leutheusser, H.J., "Plane-Couette flow between smooth and rough walls," Experiments in Fluids, vol. 11, pp. 302–312, 1991.
3. Cubit Aprepro parametrized journal files and meshes available (contact T.M. Smith).

Tasks:

1. Run different model.
2. Post process velocity profiles and compare with experimental data.

Comments and Status:

Preliminary tests have been run with SA, RNG, STD and NL models. The domain was 4hx2h. The SA model mesh was 40x80x1 with geometric stretching factor ystr=1.011, the $k-\varepsilon$ model mesh was 40x20x1 and the spacing was uniform. The top wall is moving with $U=1$. The pressure is set to zero at inlet/outlet boundaries and one node is pinned to zero to prevent the pressure from meandering. Turbulence model transport variable boundary conditions at inlet/outlets are not specified (referred to as natural or zero gradient). This has the advantage of removing free stream sensitivity to the solution. It is common to enforce periodicity on inlet/outlet boundaries, however, that option does not exist in Hydra-TH. It has been identified as an enabling capability and should be implemented in the future. Periodic BCs are robust and remove spatial bias.

The SA, STD, RNG, and NL model mean velocity profiles are compared to LES data by Kim and Menon (1997) and experimental data of Aydin and Leutheusser (1991) for $Re_h = 4762$ in the top panel of Figure 5 and $Re_h = 47,620$ in the bottom panel. Near wall spacing is indicated in the legend and the laminar solution is shown for reference. STD and RNG produce the best comparison with LES solution data. In several cases, non-asymmetry can be observed in the mean velocity profiles.

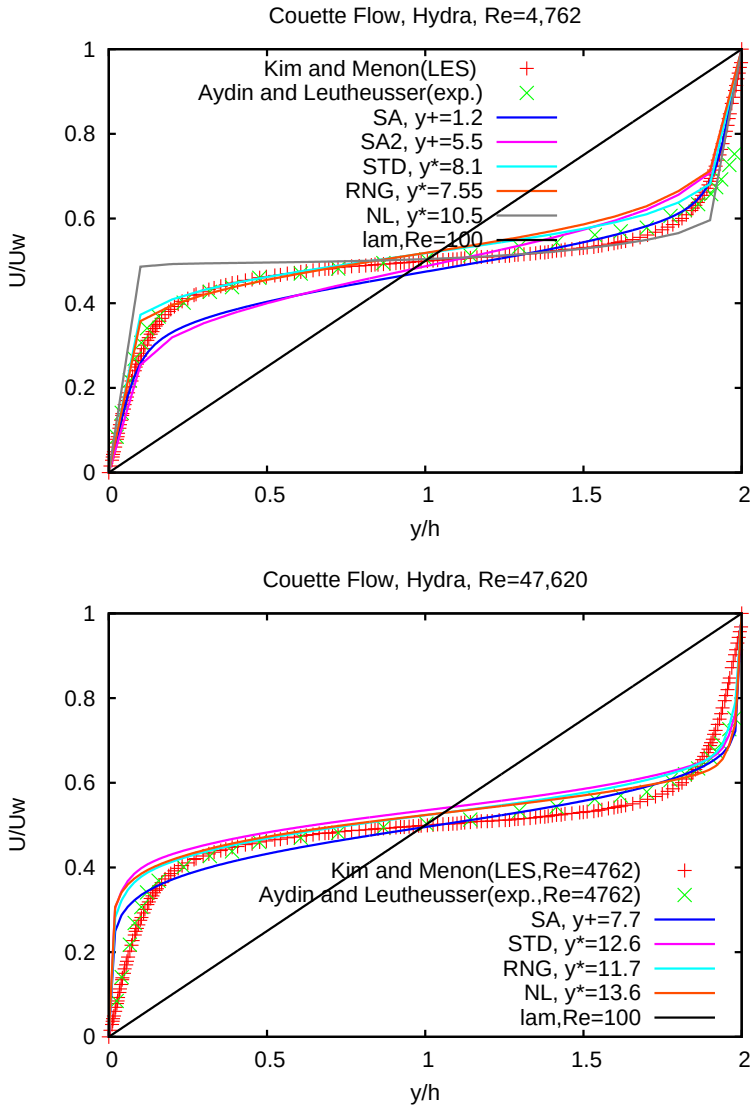

Figure 5: Couette flow mean velocity profiles at two different Reynolds numbers.

Non-asymmetry in k is seen in the top panel of Figure 6. The SA profile, bottom panel is nearly symmetric as expected. In order to remove potential bias, additional simulations were run with both walls moving. The k and ε profiles are shown in Figure 7. The single moving wall does not appear to be the source of the non-asymmetry.

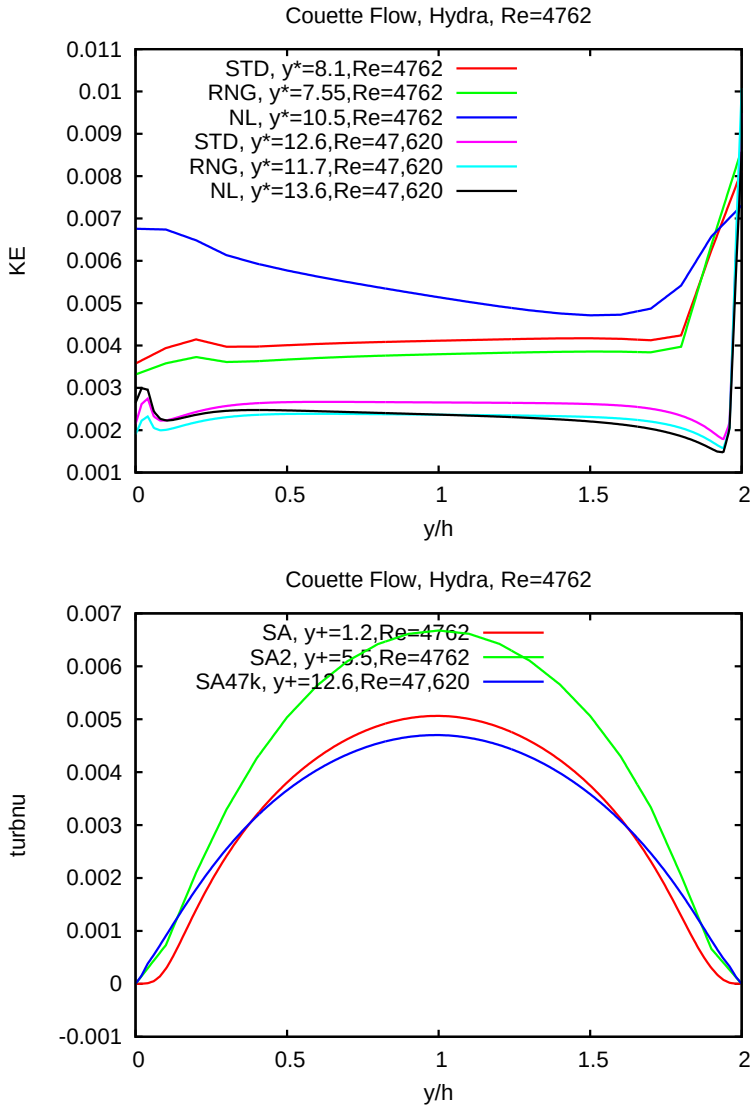

Figure 6: Couette flow turbulent kinetic energy profiles for various $k - \varepsilon$ models and $\widetilde{\nu}$ for the SA model.

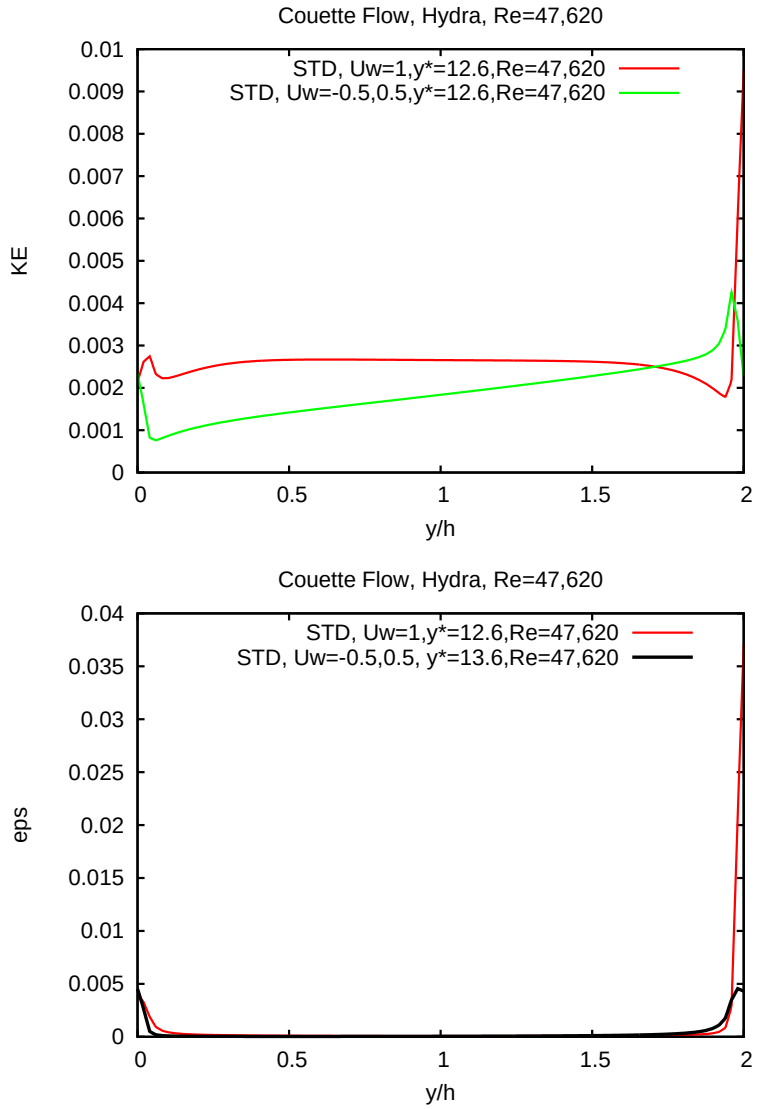

Figure 7: Couette flow turbulent kinetic energy and energy dissipation with two moving walls.

9.5 Mixing Layer

The mixing layer de-emphasizes wall modeling. It is a simple 2D benchmark problem that can be used to isolate production, dissipation, diffusion and convection mechanisms of turbulent kinetic energy and dissipation rates.

Objectives:

1. Compute the spreading rate.
2. Compare spreading rates for different models.
3. Compare profiles for scale similarity.

Resources:

1. Cubit Aprepro parametrized journal files and meshes available (contact T.M. Smith).
2. http://turbmodels.larc.nasa.gov/delvilleshear_val.html
3. Tennekes, H. and Lumley, J.L., "A First Course in Turbulence," The MIT Press, 1990.
4. F.M. White, "Viscous Flow," 2nd ed., McGraw Hill, 1991, pp. 476.
5. Rogers, M. M. and Moser, R. D., "Direct simulation of a self-similar turbulent mixing layer," Physics of Fluids, vol. 6, no. 2, pp.903–923, 1994.
6. Patel, R.P., "An Experimental Study of a Plane Mixing Layer," AIAA Journal, vol. 11, no. 1, pp. 67–71, 1973.
7. Magolan, B., Turbulent Mixing Layer.pdf (see B. Magolan).
8. Mesh and control files are available (see B. Magolan and T.M. Smith).

Tasks:

1. Conduct literature search for good quality data and/or reproducible problem description.
2. Generate meshes.
3. Setup and run.
4. Compute spreading rates.
5. Run different models.

Comments and Status:

B. Magolan has conducted a study comparing the standard model to the RNG model on a validation test provided by NASA (see url above). His study includes several different splitter

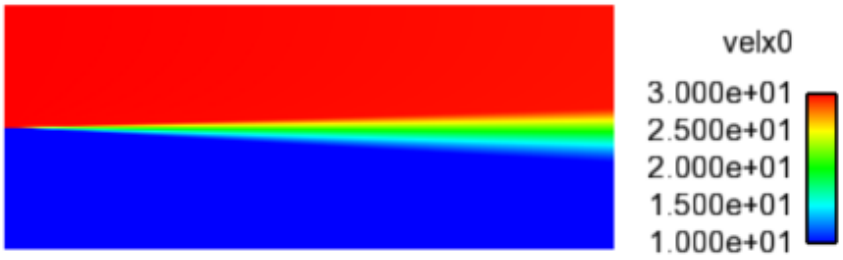

Figure 8: Mean streamwise velocity surface plot, STD $k-\varepsilon$ model.

plate geometries as well as a no-splitter plate geometry. Results include comparison of mean velocity profiles between experiment and the two turbulence models at different down-stream locations. Near the splitter plate, discrepancies are observed, possibly due to the inflow boundary layers. Far downstream, the mean velocity profiles are slightly retarded compared to experiment. The STD and RNG predict almost identical profiles far downstream. (A pdf file summarizing this study is available (see B. Magolan).

In a separate study, a simulation was conducted of a mixing layer without a splitter plate. Scale similarity in the mean velocity is expected when the Reynolds number based on velocity difference and distance from the splitter plate $Re_x = \Delta U x/\nu = 4 \times 10^5$ (Tennekes and Lumley, pp. 129). For this study, the high speed velocity was $U2 = 30\ m/s$, the low speed velocity was $U1 = 10\ m/s$, the kinematic viscosity was $\nu = 1.0e-5\ m^2/s$, density was $\rho = 1\ kg/m^3$, and the domain size was $Lx \times Ly \times Lz = 0.5 \times 0.2 \times 0.001\ m$. The SA, STD, and RNG model meshes were 500x300x1 and the geometric stretching factors were strx=1.005 and stry=1.02. The RKE model mesh was 300x100x1 with strx=1.01 and stry=1.07. A second mesh, used in the RKE simulations, was necessary because steady-state convergence could not be achieved with the finer mesh. The inlet turbulent kinetic energy boundary condition on the upper faster stream was $k = 0.03375\ m^2/s^2$ and on the lower slower stream $k = 0.00375\ m^2/s^2$. The energy dissipation boundary condition was not specified (referred to as natural or zero gradient). On upper and lower surfaces, zero penetration was assumed. At the outflow, the pressure was set to zero and on the front and back (z-planes), symmetry conditions were prescribed.

A solid contour plot of streamwise velocity is shown in Figure 8. Profiles were extracted at x=0.25, 0.35, 0.45 m for SA, STD, RNG and RKE models. The profiles are normalized according to White (pp. 476),

$$u^* = \frac{(\tilde{u} - U1)}{(U2 - U1)} \quad \delta = \frac{(U2 - U1)}{(\partial \tilde{u}/\partial y|_{max})}. \tag{9}$$

Figure 9 shows the normalized profiles at the three locations for the four different models. Scale similarity is observed for all four models. A next step, that has not been completed is to measure the spread angle and compare with experimental data.

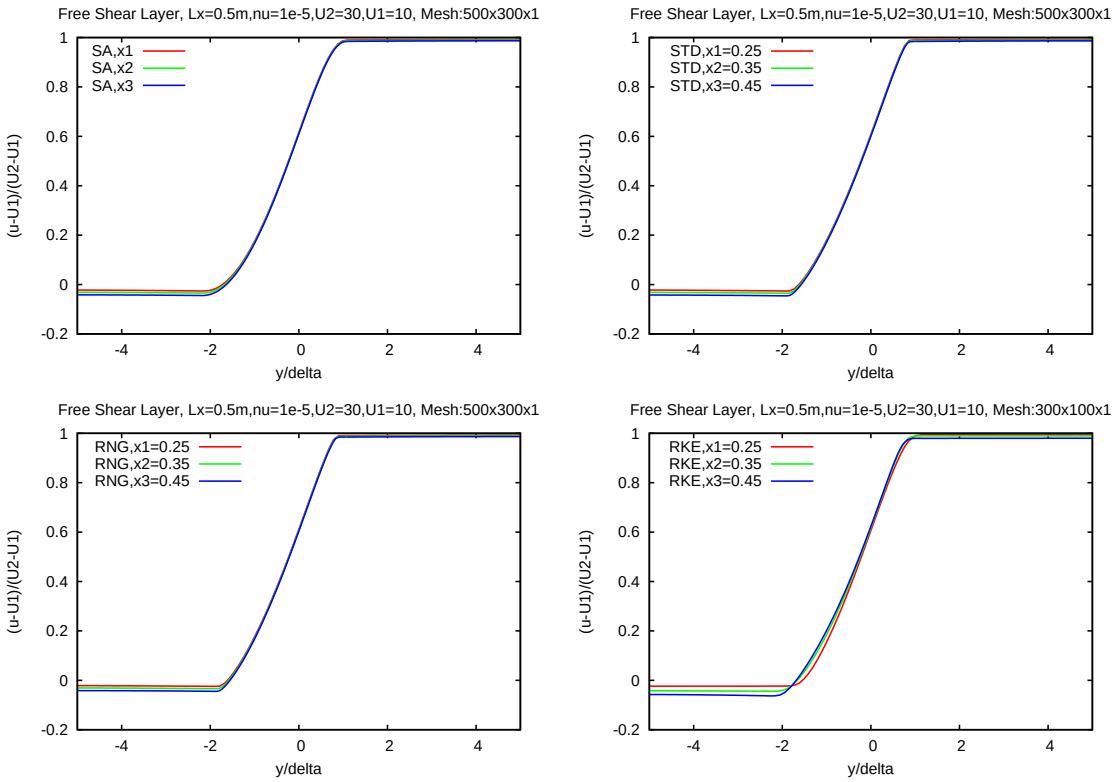

Figure 9: Scaled velocity profiles at three streamwise locations in a mixing layer without splitter plate, SA, STD, RNG and RKE models.

9.6 Planar and Round Jets

The planar and round jet de-emphasizes near wall modeling. It is a simple 2D and 3D benchmark problems that can be used to isolate production, dissipation, diffusion and convection mechanisms of turbulent kinetic energy and dissipation rates. In addition, there is a well known spreading rate anomaly comparing planar versus round jet solutions that is mainly due to the dissipation rate equation ε [30]. The spreading of round jets is always smaller than the planar jet but model predictions usually contradict this observation.

Objectives:

1. Compute the spreading rate.
2. Compare the different models.

Resources:

1. Shih et al., "A New $k-\varepsilon$ Eddy Viscosity Model for High Reynolds Number Turbulent Flows," Computers and Fluids, 1995.

Tasks:

1. Conduct literature search and choose appropriate references with good quality data and reproducible setups.
2. Generate meshes.
3. Setup and run.
4. Compute spreading rates.
5. Run different models.

Comments and Status:

Work has not started on this test problem yet.

9.7 Fully Developed Flow in Circular Pipes

Objectives:

1. Compute y^+ vs. U^+.
2. Compute Nusselt number with different models.
3. Obtain consistency between side set output delegate data, boundary conditions and solution.

Resources:

1. F. M. White. Viscous Fluid Flow, 1991.
2. S.B. Pope. "Turbulent flows," 2000.
3. Kays and Crawford, "Convective Heat and Mass Transfer, 3rd ed.," 1993.
4. Smith, T.M. et al., "Thermal Hydraulic Simulations, Error Estimation and Parameter Sensitivity Studies in Drekar::CFD," CASL L3:THM.CFD.P7.05, 2013.
5. Zagarola, M. V. and A. J. Smits, "Mean-flow scaling of turbulent pipe flow." Journal of Fluid Mechanics 373: 33-79, 1998.
6. Zagarola, M. V. and A. J. Smits, "Scaling of the Mean Velocity Profile for Turbulent Pipe Flow." Physical Review Letters 78(2): 239-242, 1997.
7. Cubit meshes are available for this problem (contact T.M. Smith).

Tasks:

1. Setup control files and run.
2. Compute law-of-the-wall and Nusselt number for different RANS models.
3. Document post-processing.
4. Run additional models.

Comments and Status:

The non-dimensional wall normal distance y^+ and velocity U^+ are determined from the wall shear τ_w and kinematic viscosity ν;

$$y^+ = u_\tau y/\nu \quad u_\tau = \sqrt{\frac{\tau_w}{\rho}} \quad U^+ = \frac{u(y)}{u_\tau}.$$

In the viscous sub-layer of a boundary layer, viscous forces dominate and velocity fluctuations are damped due to viscosity and close wall proximity. The mean velocity scales as

$$U^+ \approx y^+$$

Away from the wall, the law-of-the-wall describes the mean velocity by

$$U^+ = \frac{1}{0.41}\ln(y^+) + 5.2. \tag{10}$$

In unstructured meshes the wall shear is estimated as

$$\begin{aligned} (S_{ij})_w &= \frac{1}{2}\left(\frac{\partial v_i}{\partial x_j} + \frac{\partial v_i}{\partial x_j}\right)_w \\ t_i &= 2\mu(S_{ij})_w n_j \\ s_i &= t_i - (n_j t_j) n_i \\ \tau_w &= \sqrt{s_i s_i} \end{aligned} \tag{11}$$

where t_i is the traction vector, n_i is a unit vector normal to the surface and s_i is the shear-traction vector. A difficulty arises in estimating wall shear $(S_{ij})_w$ when using a wall function with the y^+ of the first cell $y^+ \geq 11$ because the finite-difference of the wall normal gradient is not accurate due to the coarse resolution normal to the wall imposed on the mesh by the wall model.

Kays&Crawford[22] (p. 249, Equation 12-14) present an equation for determining the shear velocity (attributed to Petukhov [29])

$$cf/2 = (2.236\ \ln(Re_D) - 4.639)^{-2} \qquad u_\tau = V\sqrt{cf/2}. \tag{12}$$

The Nusselt number Nu is a non-dimensional number that represents the ratio of convective to conductive heat transfer. For fully developed pipe flow, it is defined as

$$Nu = \frac{hD}{\kappa} \tag{13}$$

where h is the local convection heat transfer coefficient, D is a reference length scale which in this case is the pipe diameter and κ is the thermal conductivity coefficient. The mean temperature or mixing temperature T_m is the average temperature of a cross-section of the pipe and is defined as;

$$T_m = \frac{1}{\rho V A}\int_A \rho \mathbf{u}\cdot\mathbf{n} T dA \tag{14}$$

where A is the cross-sectional area, V is the average axial component of velocity defined as;

$$V = \frac{1}{\rho A}\int_A \rho \mathbf{u}\cdot\mathbf{n} dA \tag{15}$$

$\mathbf{u}$ is the velocity vector at a point on the surface and $\mathbf{n}$ is a unit vector normal to the surface. Newton's law of cooling can be stated as;

$$\dot{q}''_w = h(T_w - T_m) \tag{16}$$

where $\dot{q}''_w$ is the wall heat flux. The average wall heat flux in this case is defined by a line integral around the circumference of the pipe wall;

$$\dot{q}''_w = \frac{1}{L}\oint_L \kappa \frac{\partial T}{\partial \mathbf{n}} dl. \tag{17}$$

In this case $\frac{\partial T}{\partial \mathbf{n}}$ is the temperature gradient normal to the wall and tangent to the surface for which the flux is computed and the integration is a line traversing the circumference of the tube. In a similar way, the local (axial location) reference wall temperature is computed as;

$$T_w = \frac{1}{L}\oint_L T dl. \tag{18}$$

The final definition of Nu is;

$$Nu = \frac{hD}{\kappa} = \frac{\dot{q}''_w D}{\kappa(T_w - T_m)}. \tag{19}$$

For Prandtl number near unity, Reynold's analogy states that the temperature profile will be similar to the velocity profile [22] (p. 280), thus,

$$\frac{\bar{u}}{\bar{u}_c} = \left(1 - \frac{r}{r_w}\right)^{1/7} \qquad \frac{\bar{T} - T_w}{\bar{T}_c - T_w} = \left(1 - \frac{r}{r_w}\right)^{1/7}, \tag{20}$$

where $\bar{u}_c$ and $\bar{T}_c$ are centerline values to velocity and temperature respectively. Using this assumption and the assumption that $Pr_t \approx 1.0$, Kays&Crawford [22] present correlations for Nusselt number ($Nu = Nu(Re_D, Pr)$) (Equation 14-7) for constant wall heat flux

$$Nu = 0.022\ Pr^{0.5}\ Re_D^{0.8} \qquad Re_D < 10^5 \tag{21}$$

and for constant wall temperature (Equation 14-12)

$$Nu = 0.021\ Pr^{0.5}\ Re_D^{0.8} \qquad Re_D < 10^5. \tag{22}$$

The thermal entry length for turbulent flow is much longer than the laminar case. It is estimated from Kays&Crawford that for $\frac{x}{D} = 20$, the length of the computational domain, the error in Nu is approximately 2% ([22] p. 340-341).

Fully developed pipe flow is achieved by specifying a constant pressure at inflow and outflow boundaries. The pressure gradient drives the development of the flow. At steady-state, there should be no axial variation in any of the flow variables. All three Reynolds numbers for SA, STD and RNG model simulations were created by varying the pressure at inlet and outlet. This problem has the added advantage that the turbulence variables at the inlet and outlet are computed as part of the solution. It is common to enforce periodicity on inlet/outlet boundaries, however, that option does not exist in Hydra-TH. It has been identified as an enabling capability and should be implemented in the future. Periodic BCs are robust and remove spatial bias.

The pipe diameter was $D = 0.01\ m$, computational length was $x = 20D$, density was constant $\rho = 1\ kg/m^3$ viscosity was $\mu = 1.0E-6\ kg/ms$, and the mesh contained 167,936 elements. The numerical tests were conducted with $Pr = Pr_t = 1.0$. Both constant wall temperature and constant wall heat flux boundary conditions were investigated. In the case of constant heat flux boundary condition, the wall temperature is determined from Equation 7. A single mesh like the one shown in Figure 10 was used for all SA simulations and second mesh was used for all of the $k-\varepsilon$ simulations. The mesh requirements in the near wall region are different for SA and $k-\varepsilon$ models. The SA model requires $y^+ \approx 1$ and the y*-insensitive model works best if $y^* \approx 20-30$.

Mean velocity profiles and scaled velocity profiles for the SA model are shown in Figure 11. From Table 3 $y^+ \leq 6.1$ for all three Reynolds numbers and the scaled velocity profiles capture the law-of-the-wall. In the case of the STD model, a much coarser mesh is required by the y*-insensitive wall function and for this reason, using finite-difference to compute the wall shear stress is inaccurate. This can be seen in the left panel of Figure 12. In the legend, "fd" refers to finite-difference and "Hydra" refers to Equation 3. Using Hydra-THs' output delegate gives a better estimate of τ_w than finite-difference however, is still not satisfactory. Finally, if Equation 12 is used scaled velocity captures the law-of-the-wall as seen on the right panel of Figure 12. Note that the entire viscous-sublayer is missing in the simulations. This is due to the assumption built into the wall function that the first integration point

should lie outside the viscous sublayer. A similar result is observed for the RNG model, Figure 13.

Table 3 contains a summary of comparisons of wall heat flux. The column labeled "BC" refers to using the boundary condition value for the heat flux in Equation 19, "Calculated" refers to computing heat flux using a finite-difference procedure and "Side Set" refers to using Hydra-THs' surface output delegate values. The fact that the three values are different emphasizes the point that care must be taken when estimating surface quantities like Nu.

Nusselt number predictions for both constant wall temperature and constant wall heat flux computed from solutions using the SA model are shown on Figure 14. Computed values are compared with correlations by Kays&Crawford [22], Equation 21.

In the legend, "calc" refers to finite-difference based estimate of heat flux, "Hydra" refers to it's output delegate and "ref." refers to using the boundary condition value.

The Spalart-Allmaras model produces accurate Nu for both constant wall temperature and constant wall heat flux cases when the heat flux is calculated by the post-processing procedure. The Hydra-TH sideset output delegate values are inconsistent with the post-processed values. The reference heat flux for the Nusselt number calculations for the case of constant heat flux wall boundary condition is the boundary value itself specified in the control file. The Hydra-TH sideset value is the line integrated average (Equation 17) of the values written to the exodus surface delegate in the plot file. These values are not necessarily the same. When the reference value is used to compute Nusselt number the agreement with the correlations is satisfactory. On the other hand, for the case of constant wall temperature, the Nusselt numbers computed using the Hydra-TH sideset values are more accurate than the Nusselt numbers computed by the post-processing procedure. Indeed, the effective conductivity due to the y*-insensitive wall model somewhat compensates for the coarse mesh which cannot resolve the temperature gradient at the wall.

Model	V	ΔP	Re_D	y^+ or y^*	BC T_w or $\dot{q}''_w$	Calculated $\dot{q}''_w$	Side Set $\dot{q}''_w$
SA	1.97	1.0	19,743	$y^+ = 1.73$	$T_w = 350$	222.69	212.47
SA	4.23	4.0	42,269	$y^+ = 3.44$	$T_w = 350$	432.97	414.50
SA	8.23	14.0	82,291	$y^+ = 6.04$	$T_w = 350$	729.41	719.26
SA	1.97	1.0	19,743	$y^+ = 1.73$	$\dot{q}''_w = 250$	256.33	85.62
SA	4.23	4.0	42,269	$y^+ = 3.44$	$\dot{q}''_w = 250$	253.42	83.71
SA	8.23	14.0	82,291	$y^+ = 6.04$	$\dot{q}''_w = 250$	231.37	69.36
RNG	1.96	1.0	19,612	$y^* = 15.02$	$T_w = 350$	77.93	187.57
RNG	4.23	4.0	42,268	$y^* = 30.97$	$T_w = 350$	95.54	331.24
RNG	8.45	14.0	84,522	$y^* = 58.89$	$T_w = 350$	109.39	556.88
RNG	1.96	1.0	19,612	$y^* = 15.02$	$\dot{q}''_w = 250$	75.72	18.16
RNG	4.23	4.0	42,268	$y^* = 30.97$	$\dot{q}''_w = 250$	51.24	12.66
RNG	8.45	14.0	84,522	$y^* = 58.89$	$\dot{q}''_w = 250$	34.49	9.67

Table 3: Fully developed turbulent pipe flow, wall heat flux.

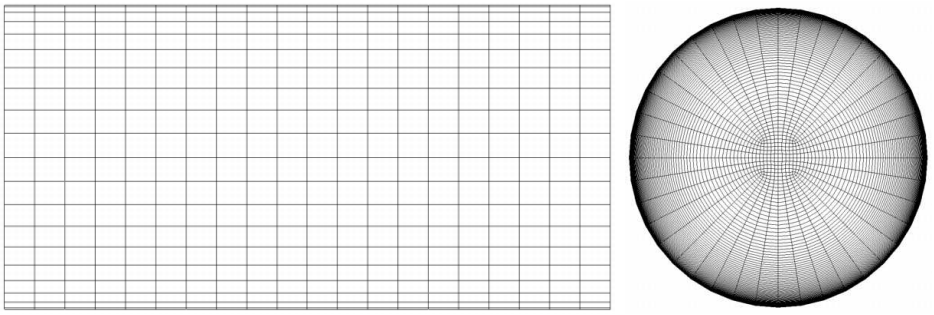

Figure 10: Fully developed pipe flow computational mesh with 62,000 elements, truncated in z-direction.

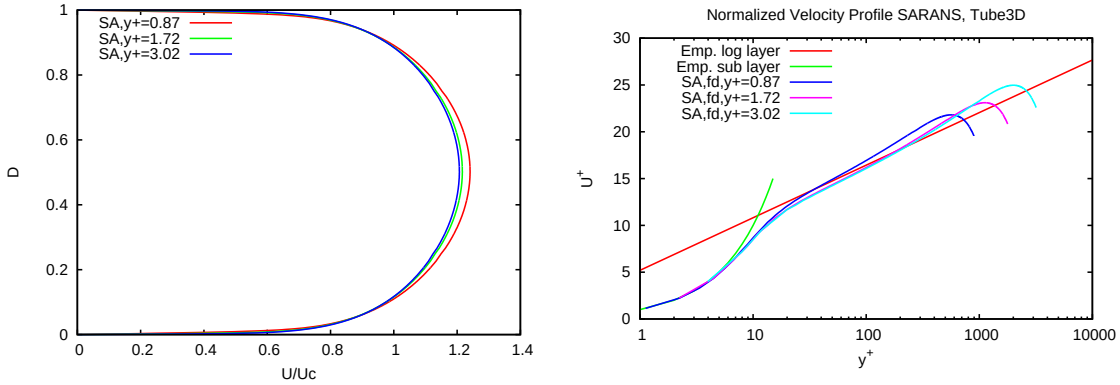

Figure 11: Fully developed pipe flow law of the wall for SARANS.

Nusselt number predictions for the STD model are presented in Figure 15. For constant wall temperature, wall heat flux is computed four ways; calculated with finite-difference, Hydra-TH output delegate, Equation 5 and Equation 1. The output delegate and Equation 5 using similar formulations, produce similar results while finite-difference and Equation 1 under-estimate Nu.

For constant heat flux, a fifth way using the boundary condition reference value is included. In this case, the reference value over-estimates Nu while Equation 5 agrees well with Equation 21. The Nusselt number is under-estimated when a finite-difference, output delegate or Equation 1 is used. For constant temperature, Hydra-TH output delegates produced accurate Nu while for constant heat flux output delegates were not accurate. This seems inconsistent and warrants further investigation.

Similar results to the STD model were obtained with the RNG model.

This problem serves as good validation test for low-Re near wall model extensions and wall functions. As can be seen in the plots, the Spalart-Allmaras model solutions capture the viscous sub-layer. Also, when properly interpreted, the wall functions also produce accurate Nu. This simple turbulent heat transfer problem demonstrates that more work is needed on Hydra-TH output delegates to ensure accurate surface quantities are computed.

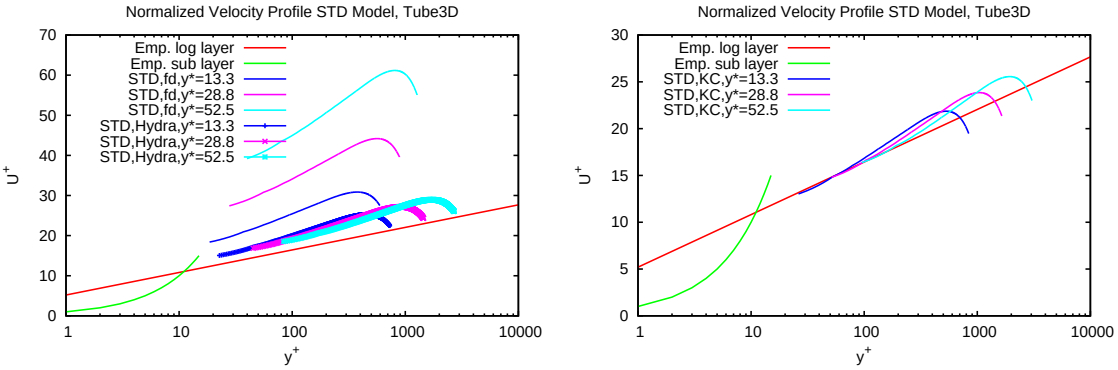

Figure 12: Fully developed pipe flow law of the wall for STD.

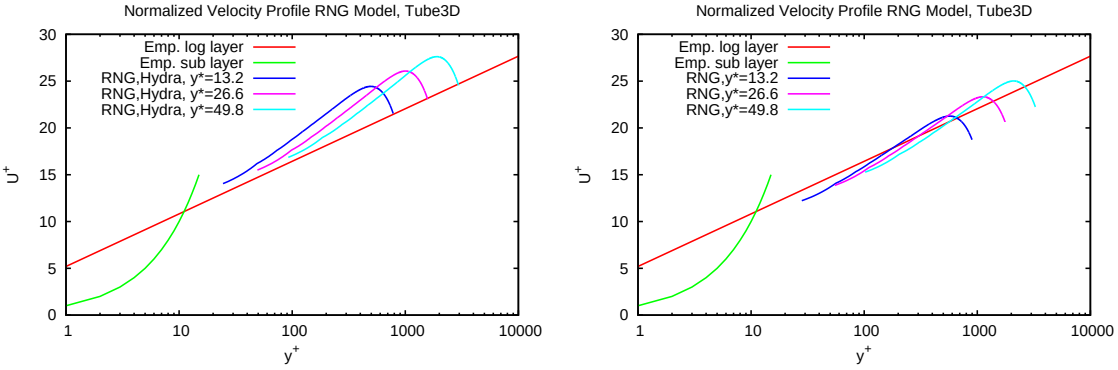

Figure 13: Fully developed pipe flow law of the wall for RNG.

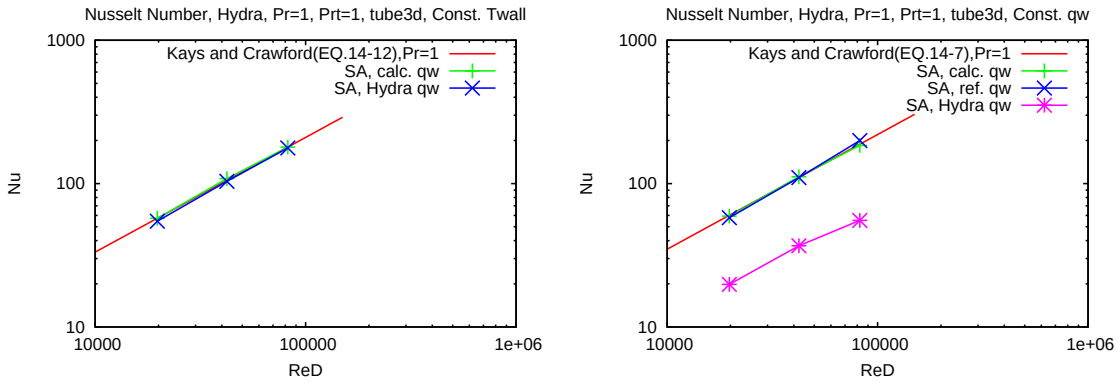

Figure 14: The Nusselt number for SARANS with constant wall temperature and constant wall heat flux.

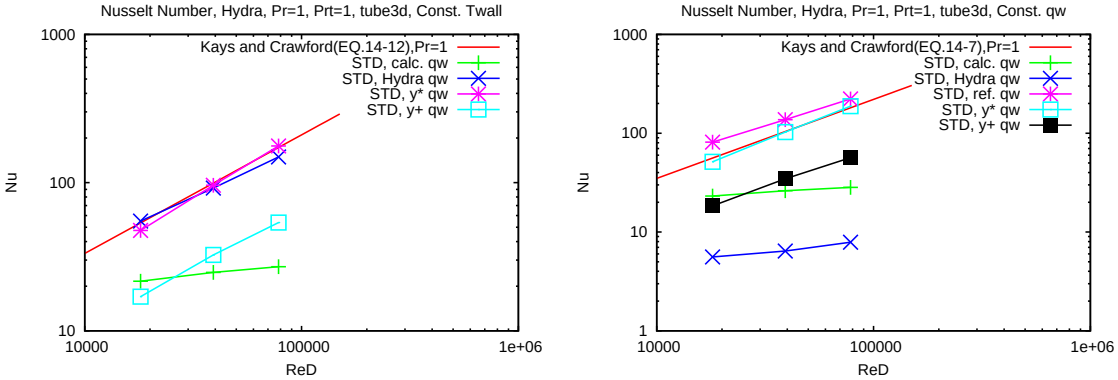

Figure 15: The Nusselt number for STD with constant wall temperature and constant wall heat flux.

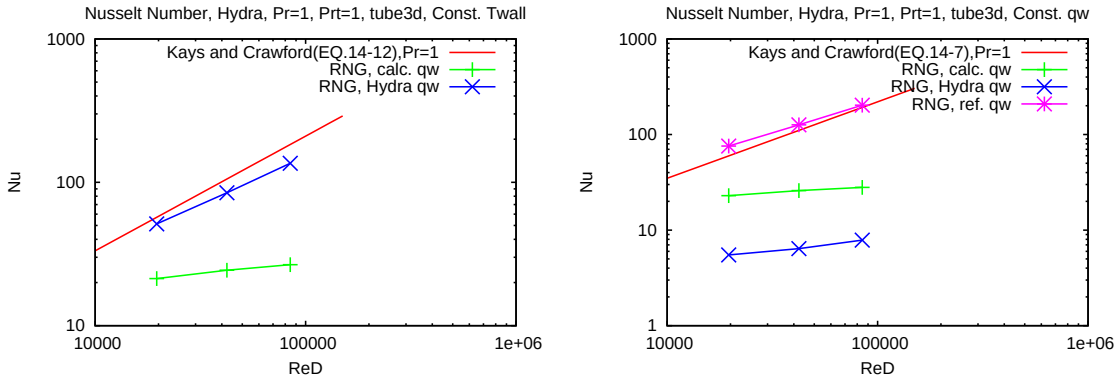

Figure 16: The Nusselt number for RNG with constant wall temperature and constant wall heat flux.

9.8 U-Channel Flow

Objectives:

1. Assess the rotation/curvature correction of Dacles-Mariani et al. applied to the Spalart-Allmaras model.
2. Assess RANS models in general under high geometric curvature.

Resources:

1. Spalart, P.R. and Shur, M. "On the Sensitization of Turbulence Models to Rotation and Curvature," Aerospace Science and Technology, no. 5, 1997.
2. M.L. Shur et al. "Turbulence Modeling in Rotating and Curved Channels: Assessing the Spalart-Shur Correction," AIAA J., 2000.
3. P.E. Smirnov and F. R. Menter. "Sensitization of the SST Turbulence Model to Rotation and Curvature by Applying the Spalart-Shur Correction Term," Journal of Turbomachinery, 2009.
4. Dacles-Mariani, J. et al. "Numerical/Experimental Study of a Wingtip Vortex In the Near Field," AIAA Journal vol. 33, 1995.
5. Dacles-Mariani, J. et al., "On Numerical Errors and Turbulence Modeling in Tip Vortex Flow Prediction," IJNMF, vol. 30, 1999.
6. "Enhanced Turbulence Model Capabilities in Hydra-TH," Smith, T.M. and Christon, M.A., CASL L3:THM.CFD.P9.06, 2014.
7. Cubit meshes are available for this problem (contact T.M. Smith).

Tasks:

1. Run additional models.
2. Document in V&V manual.
3. Document post-processing.

Comments and Status:

This was studied extensively and reported in [32]. To evaluate this correction, we investigated its performance in a two-dimensional U-channel flow that has a 180 degree bend. The U-channel was investigated experimentally and numerically by Monson et al. [26] and also numerically by Shur et al. [31] in the context of their version of a rotation/curvature correction. A comparison of solutions using both uncorrected and corrected versions of SA were compared.

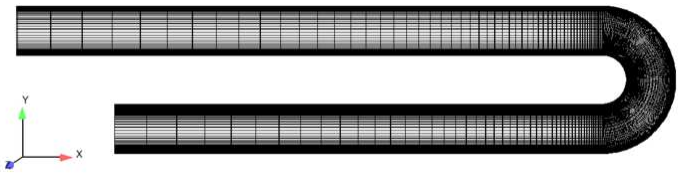

Figure 17: The computational mesh for 204x111 resolution.

An example of a computational mesh that also illustrates the geometry is shown in Figure 17. Flow enters at the lower left boundary and the exits upper right. The bend is a half circle. The inlet is located at $s/H = -10$, the start of the bend at $s/H = 0$, the end of the bend is at $s/H = \pi$ and the outflow is at $s/H = 12 + \pi$. Skin friction and pressure coefficients have been plotted in terms of arc length (s/H) normalized by channel height H, measured from the inlet to the exit along the center line of the channel for both outer and inner walls and are presented in [32]. Predictions of velocity profiles at four stations for the corrected/uncorrected Spalart-Allmaras and RNG $k - \varepsilon$ models are presented in [32].

9.9 Flow Over a Circular Cylinder

Objectives:

1. Compute Strouhal number.
2. Investigate URANS modeling strategy.

Resources:

1. M. Tutar and A. E. Holdo, "Computational modeling of flow around a circular cylinder in sub-critical flow regime with various turbulence models," IJNMF, 2001.
2. A. Travin et al., "Detached-Eddy Simulations Past a Circular Cylinder," Flow, Turbulence and Combustion, 1999.
3. P. Catalano et al., "Numerical simulation of the flow around a circular cylinder at high Reynolds numbers," Int. J. of Heat and Fluid Flow, 24, 2003.
4. Cubit meshes are available for this problem (contact T.M. Smith).

Tasks:

1. Choose the range of Reynolds numbers.
2. Generate Cubit meshes from journal files.
3. Compute Strouhal number from probe data and computed spectrum.
4. Run different models.

Comments and Status:

This problem is a regression test for SA and RNG $k-\varepsilon$ models. These tests will serve as a starting point for more detailed studies including additional models.

9.10 Flow over a Triangular Cylinder

Objectives:

1. Compute Strouhal number.
2. Investigate URANS modeling strategy.

Resources:

1. P. A. Durbin, "Separated Flow Computations with the k-e-v2 Model," AIAA J., 1995.
2. Johansson, S., Davidson, L., and Olsson, E., "Numerical Simulation of the Vortex Shedding past Triangular Cylinders at High Reynolds Number Using a k-s Turbulence Model," International Journal of Numerical Methods in Fluids, Vol. 16, No. 6, 1993, pp. 859-878.

Tasks:

1. Generate meshes.
2. Setup control files and run.
3. Run different models.

Comments and Status:

Work has not started on this problem yet.

9.11 Flow over a Square Cylinder and Rounded Corner Cylinder

Objectives:

1. Compute Strouhal number.
2. Investigate URANS modeling strategy.

Resources:

1. D. A. Lyn, et al., "A laser-doppler velocimetry study of ensemble-averaged characteristics of the turbulent near wake of a square cylinder," J. Fluid Mech., 1995.

2. G. Bosch and W. Rodi, "Simulation of Vortex Shedding Past a Square Cylinder with Different Turbulence Models," IJNMF, 1998.

3. K. D. Squires et al., "Detached-Eddy simulation of the separated flow over a rounded-corner square," Journal of Fluids Engineering, 2005.

Tasks:

1. Generate meshes.

2. Setup control files and run.

3. Run different models.

Comments and Status:

Work has not started on this problem yet.

9.12 Flow in an Asymmetric Diffuser

Objectives:

1. Investigate pressure gradient induced separation.

Resources:

1. C. U. Buice and J. K. Eaton, "Experimental Investigation of Flow Through an Asymmetric Plane Diffuser," Journal of Fluids Engineering, 2000.

2. H. J. Kaltenbach et al., "Study of flow in a planar asymmetric diffuser using large-eddy simulation," J. Fluid Mech, 1999.

3. http://www.grc.nasa.gov/WWW/wind/valid/buice/buice.html

Tasks:

1. Generate meshes.

2. Setup control files and run.

3. Run different models.

Comments and Status:

Work has not started on this problem yet.

9.13 Impinging Jet Flow

Objectives:

1. Prediction of Nusselt number in stagnation point flows.
2. Assess calculation of surface quantities of interest from flow solutions.

Resources:

1. M. Hadziabdic and K. Hanjalic, "Vortical structures and heat transfer in a round impinging jet," J. Fluid Mech., 2008.
2. Banjec, M. and Vasiljevic, B., "Development of a new Near-wall Reynolds Stress Turbulence Model for Jet Impingement Heat Transfer Prediction," FME Transactions, vol. 32, pp. 69–6, 2004.
3. Cooper, D., Jackson, D.C., Launder, B.E. and Liao, G.X., "Impinging jet studies for turbulence model assessment -I. Flow field Experiments," International Journal of Heat and Mass Transfer, vol. 36, no. 10, pp 2675–2684, 1993.
4. Craft, T.J., Graham, J.W. and Launder, B.E., "Impinging jet studies for turbulence model assessment -II. An examination of the performance of four turbulence models," International Journal of Heat and Mass Transfer, vol. 36, no. 10, pp 2685–2697, 1993.
5. Craft, T.J., Launder, B.E. and Suga, K., "Development and application of a cubic eddy-viscosity model of turbulence," International Journal of Heat and Fluid Flow, vol. 17, no. 2, pp 108–115, 1996.
6. Behnia, M., Parneiz, S. and Durbin, P.A., "Prediction of heat transfer in an axisymmetric turbulent jet impinging on a flat plate," International Journal of Heat and Mass Transfer, vol. 41, no. 12, pp. 1845–1855, 1998.
7. Kubacki, S. and Dick, E. "Hybrid RANS/LES of Low Reynolds Number Round Impinging Jets," V European Conference on Computational Fluid Dynamics, ECCOMAS CFD 2010.
8. Cubit meshes are available from T.M. Smith for the quarter and full geometry.

Tasks:

1. Generate meshes.
2. Setup control files and run.
3. Run different models.
4. May require LES.
5. Compare RANS to LES solutions.

Comments and Status:

An axisymmetric cold turbulent jet impinging on a circular hot wall with constant heat flux is analyzed using steady RANS simulations. Hydra-TH solves the three-dimensional equations and therefore the smallest geometry that can represent this flow is one quadrant of a circle. Flow conditions were; bulk jet exit velocity $V_z = 1.0\ m/s$, density, $\rho = 1\ kg/m^3$, specific heat $C_p = 1000\ J/kgK$, Reynolds number based on pipe diameter $Re_D = 23,000$, Prandtl number $Pr = 0.71$, turbulent Prandtl number $Prt = 0.85$, $H/D = 2$, $R/D = 8$, entrainment velocity $V_{entrain} = 0.01V_z$, outflow pressure $P_{out} = 0\ Pa$. $T_{jet} = 300\ c$, $\dot{q}''_w = 250\ W/m^2$, $\mu = 4.3478e-5\ kg/ms$ and $\kappa = 0.061237\ W/mK$. The domain including the pipe and region outside the pipe were extended by an amount $-H$ above the pipe exit. This allows the flow in the pipe to develop from a prescribed power law velocity and uniform k profiles, and lessens the effect of the top boundary on the flow near the hot plate. It should be noted that in most published work, a separate pipe flow simulation is performed and the solution is then transferred to the impinging jet inlet, thus providing more realistic flow conditions at the pipe exit. The SA model small mesh contained 407,040 and large mesh 637,440 (lm) elements. The $k-\varepsilon$ model mesh contained 280,320 elements. Simulations were run with the fully-implicit solver and CFLmax=100. The total kinetic energy history for various models is shown in Figure 18 which is used to determine whether steady-state has been achieved. An example of the velocity flow field is shown in Figure 19. The flow impinging on the plate creates a stagnation region and then forms a radial boundary layer flow along the plate.

The Nusselt number (Nu) for various models are shown in Figure 20. The Nu is defined as (see § 9.7)

$$Nu = \frac{hD}{\kappa} = \frac{\dot{q}''_w D}{\kappa(T_w - T_m)} \tag{23}$$

where the mixing temperature T_m is the average temperature at the pipe exit and is easily computed, and D is the pipe diameter. It is much more difficult to estimate the wall heat flux and wall temperature. Simulations using the SA model require grids that produce $y^+ \approx 1$. Table 4 give estimates for y^+ and y^*, the scale used by $k-\varepsilon$ wall function models. Since $U^+ \approx y^+$ in the viscous sublayer ($y^+ < 11.225$) the wall heat flux can be accurately computed using a finite-difference approximation and the the wall temperature can be estimated by taking into account the value of temperature in the cell adjacent to the wall and the wall heat flux, Equation 7.

Model	Scale	Range	Average
SA	y^+	0.17-1.1	0.85
STD	y^*	3.6-21	17
RNG	y^*	3.8-13	11
NL	y^*	5.0-17	14

Table 4: Estimates for y^+ and y^* for the impinging jet flow.

Comparisons of Nu with experimental data of Baughn and Shimizu shown in the top panel of Figure 20 agree well near the stagnation point, however, the SA model fails to capture the proper location of the recirculation region and therefore, the local maximum is in the wrong location. Further away from the stagnation region, the Nu is under-predicted. Several different parameters were varied in order to try improve the Nu prediction outside of

the impinging jet region, including radial mesh spacing, co-flow amplitude and the method wall heat flux and temperature were computed. In the legend; "qwref" refers to the specified boundary condition value, "calc" refers to a finite-difference approximation, "Tnode" refers to using the solution value for T_w and "Tplus" refers to using a law-of-the-wall formula, Equation 1. While in general, it can be stated that the SA model does not accurately predict Nu, it is the case that because the solution is integrated to the wall with $y^+ \approx 1$, accurate surface quantities can be extracted.

The middle panel in Figure 20 illustrates quite a different message. First, it is well known in the literature that the $k-\varepsilon$ model performs poorly in stagnating flows. This is because the jet has a potential core producing relatively little shear stress. However, the k-equation production source term has been calibrated for simple shear flows and so the normal stress over predicts the production, locally increasing k and the effective heat transport coefficient κ_{eff}. Notice that the SA model does not suffer from this issue. Second, wall functions are used for all the various $k-\varepsilon$ models with $y^* > 10$ so finite-difference approximations of surface gradients are not accurate. Wall heat flux is obtained by four methods. In addition to the those used for SA, "qwsset" refers to the output surface delegate and "qwstar" refers to Equation 5. Similarly, "Tstar" refers to Equation 5. All five Nu plots are derived from the same flow solution and algorithm for computing Nu. The differences are in how wall heat flux and temperature are computed. The (qwref,Tstar) combination produces the closest comparison with data. Just as is commonly observed, Nu in the stagnation region is over-predicted, however, the predictions improve as radial distance increases.

The bottom panel in Figure 20 compares the different model predictions to the experimental data. The NL model is a slight improvement over the other $k-\varepsilon$ models. Craft et al. [14] developed a cubic-nonlinear eddy viscosity model that accurately predicted Nu and stressed that quadratic nonlinearity was insufficient for the impinging jet.

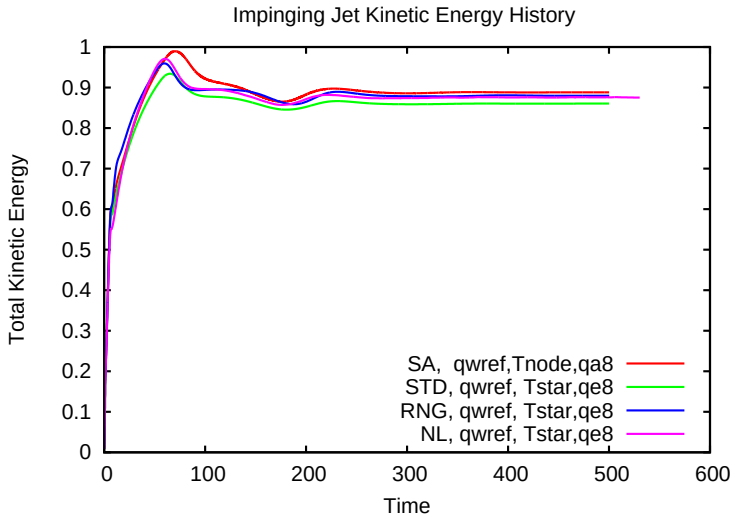

Figure 18: Impinging jet flow total kinetic energy history.

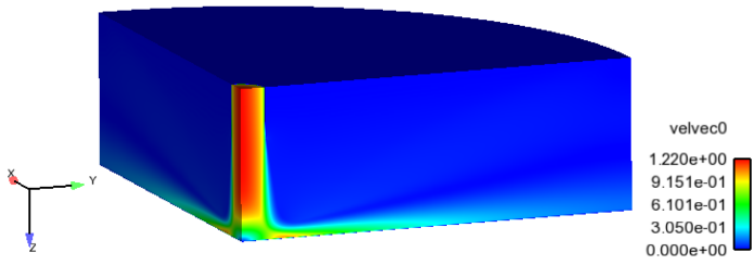

Figure 19: Impinging jet flow solid contours of velocity vector.

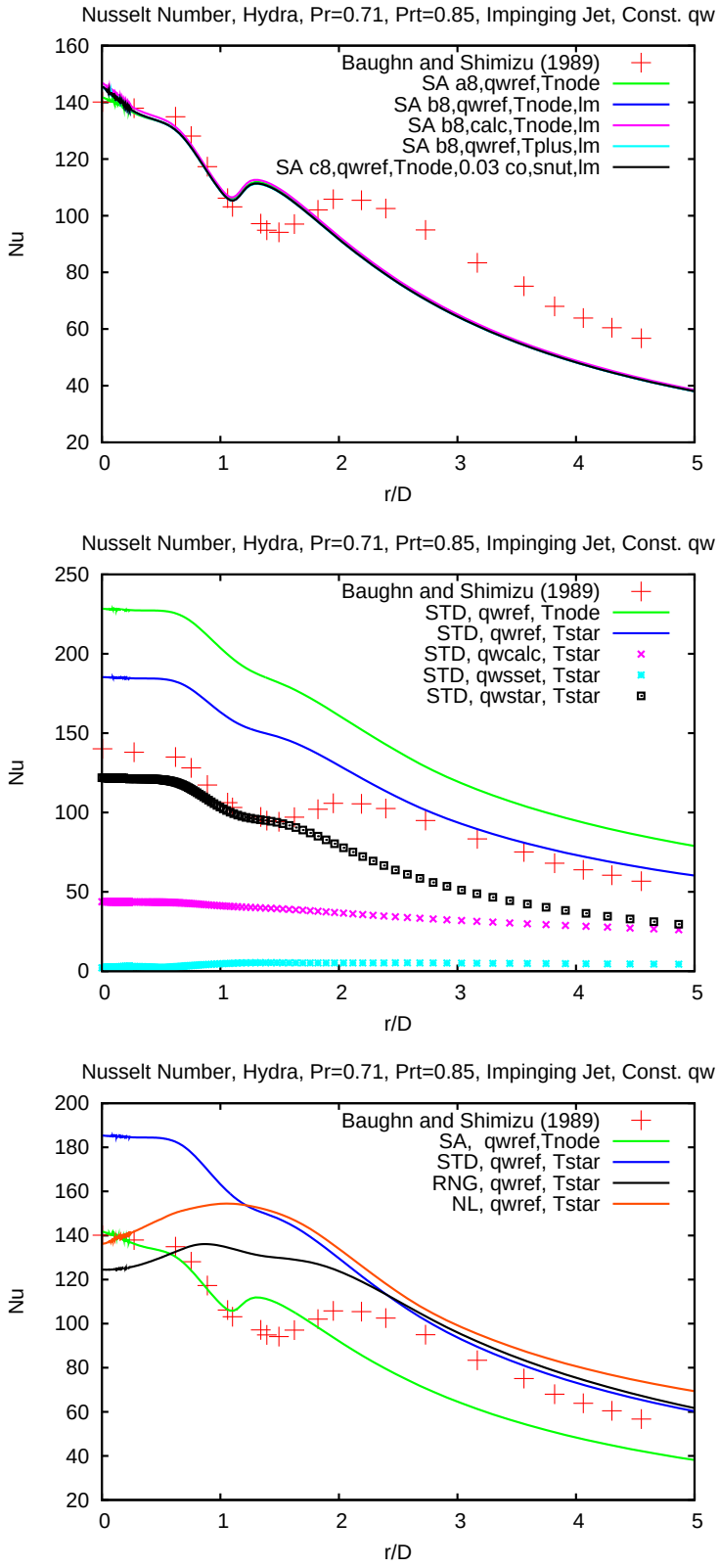

Figure 20: Impinging jet Nusselt number for; SA, STD and various models.

9.14 Jet in Crossflow

Objectives:

1. Prediction of complex vortical flows.

Resources:

1. M. R. Keimasi et al., "Numerical Simulation of Jets in a Crossflow Using Different Turbulence Models," AIAA J., 2001.

Tasks:

1. Generate meshes.
2. Setup control files and run.
3. Run different models.

Comments and Status:

Work has not started on this problem yet.

9.15 Flow over a mounted cube in a channel

Objectives:

1. Prediction of massively separated flows.
2. Investigate URANS modeling strategy.

Resources:

1. G. S. Ratnam. And S. Vengadesan, "Performance of two equation turbulence models for prediction of flow and heat transfer over a wall mounted cube," International Journal of Heat and Mass Transfer, 2008.

Tasks:

1. Generate meshes.
2. Setup control files and run.
3. Run different models.

Comments and Status:

Work has not started on this problem yet.

9.16 Square Cavity Natural Convection

Objectives:

1. Prediction of mean velocity profiles in a high Rayleigh number natural convection flow.
2. Exercise the energy equation and Boussinesq buoyancy closures.

Resources:

1. F. Ampofo and T.G. Karayiannis, "Experimental benchmark data for turbulent natural convection in an air filled square cavity," Int. J. Heat Mass Transfer 46, 3551-3572, 2003.
2. Y.S. Tian and T.G. Karayiannis, "Low turbulence natural convection in an air filled square cavity, Part I: Thermal and fluid flow fields," Int. J. Heat Mass Transfer 43, 849-866, 2000.
3. Y.S. Tian and T.G. Karayiannis, "Low turbulence natural convection in an air filled square cavity, Part II: The turbulence quantities," Int. J. Heat Mass Transfer 43, 867-884, 2000.
4. M. Omri and N. Galanis, "Numerical analysis of turbulent buoyant flows in enclosures: Influence of grid and boundary conditions," Intl. J. of Thermal Sciences 46, 727-738, 2007.
5. Cubit meshes are available from T.M. Smith.

Tasks:

1. Generate Cartesian stretched meshes.
2. Setup control files and run.
3. Run different models.

Comments and Status:

There is a discussion of this test in Pannala and Stagg [27]. This test may require conjugate heat transfer to run correctly, which is being actively developed at this time.

Update:

Simulations were designed and executed to compare with the experiments of Ampofo and Karayiannis. The computational domain was Lx=0.75, Ly=0.75 and Lz=0.1. For the STD model, three grids with uniform spacing in the x- and y-directions were used; 40x40x1, 80x80x1, 160x160x1 producing y-normal scaling $y^* = 8.4, 6.1, 3.8$ respectively. For the SA model one mesh was used with resolution 120x120x1 and geometric stretch factors strx=stry=1.046 producing $y^+ = 1.2$. Fully-implicit time integration was used and

CFLmax=25. The density was $\rho = 1.205\ kg/m^3$, heat capacity $C_p = 1005.0\ J/kgK$, viscosity was $\mu = 1.9248e-5\ kg/ms$, conductivity $\kappa = 0.027245\ W/mK$, expansion coefficient $\beta = 3.43e-3\ (1/K)$, gravity constant $g_y = -9.81\ m/s^2$, $Pr = 0.71$, $Prt = 1.0$. The left vertical wall temperature was $T_H = 50$ and the opposite wall was $T_c = 10\ c$ and the reference temperature was $T_{ref} = 30\ c$. A Boussinesq buoyancy body force was applied to the momentum and turbulent kinetic energy equations. No additional correction was added to the SA model.

Vertical velocity component contours are shown in Figure 21. A reasonable degree of asymmetry between hot, cold, upper and lower wall is observed. In Figure 22, the vertical velocity component at the midheight $y = 0.375$ for the entire length in the x-direction (top panel) and a blow-up near the hot wall (lower panel). Velocity profiles are scaled by $V_0 = \sqrt{g\beta H\Delta T} = 1$. Comparison of vertical velocity component shows reasonable agreement for SA and STD for the higher resolution mesh. It should be noted that mesh refinement for RANS models where y^+ and y^* must be maintained at certain values can be difficult.

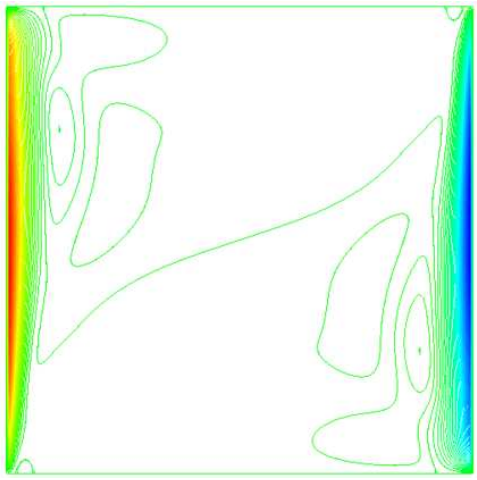

Figure 21: Vertical velocity component contours, STDKE model, 160x160x1 uniform mesh.

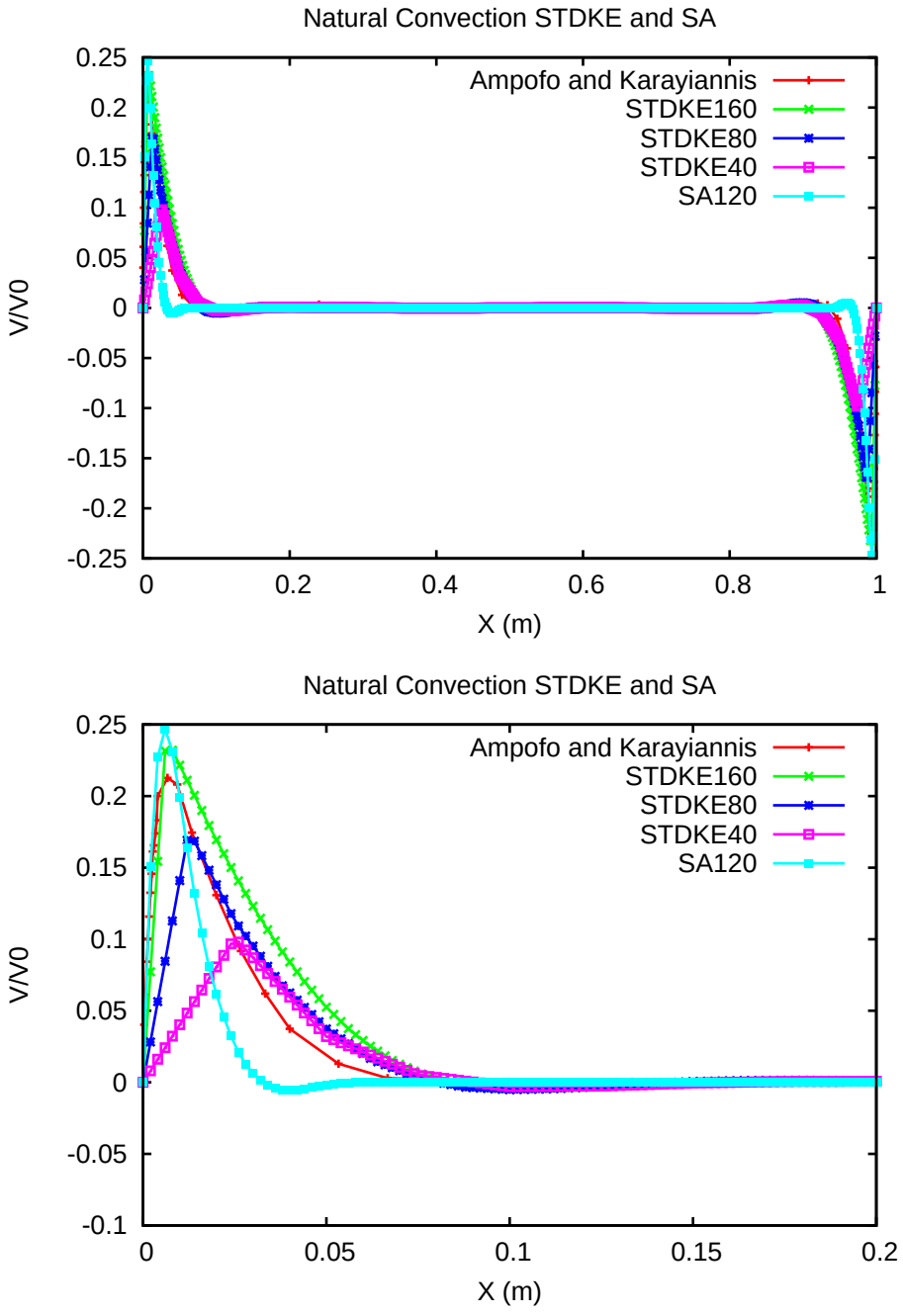

Figure 22: Comparison of vertical velocity at mid-height y=0.375; STD uniform meshes, 160x160x1, 80x80x1, 40x40x1, SA 120x120x1 stretched mesh.

9.17 Fuel Rod Sub-Channel Secondary Flow

Objectives:

1. Verify the nonlinear $k - \varepsilon$ model is working correctly.
2. Prediction of secondary flows in rod bundle reactor core sub-assembly flows.
3. Compare solutions from different models.

Resources:

1. Baglietto, "Anisotropic Turbulence Modeling of Accurate Rod Bundle Simulations," ICONE 14, 2006.
2. Magolan, B. et al., "Non-Linear Eddy Viscosity Turbulence Modeling in Hydra-TH for Fuel Related Applications," NURETH-16-13336, 2015.
3. Meshes and post-processing scripts are available for this problem (contact B. Magolan or T.M. Smith).

Tasks:

1. Rerun.
2. Post-process solutions.
3. Run different models.

Comments and Status:

Emilio Baglietto and Ben Magolan have been running these simulations in conjunction with development of the nonlinear $k - \varepsilon$ turbulence model. The current status of both the model and the simulations are documented in several Power-Point slide presentations which can be obtained from Ben Magolan or T.M. Smith. A paper detailing the use of the new model has been presented at the NURETH-16 conference August 2015.

9.18 Elmahdi 3x3 V5H Rod/Spacer Grid Reactor Core Model

Objectives:

1. Comparison of turbulence models on a CASL relevant flow problem.
2. Compute heat transfer from the rods to the flow field.
3. Compare swirling flow structure between models.
4. Compare heat transport between different models.

Resources:

1. Elmahdi, A.M. et al., "Flow induced vibration forces on a fuel rod by LES CFD Analysis," NURETH-14-365, 2011.
2. Christon, M.A. et al., "Hydra-TH L2 Milestone," LA-UR-11-07034, 2011.
3. Smith, T.M. et al., "Reactor Core Sub-Assembly Simulations Using a Stabilized Finite Element Method," NURETH-14-500, 2011.
4. Meshes are available for this problem (see T.M. Smith).

Tasks:

1. Define metrics for comparing different models.
2. Run the simulations with the different models.
3. May require LES.
4. Compare RANS to LES solutions.

Comments and Status:

This is a very important flow problem for several reasons. First, it is the closest geometry to the reactor core sub-assembly. Secondly, the geometry is very complicated and the mesh includes four different cell topologies. Finally, this problem includes heat transfer from the rods to the fluid. This will test the turbulent heat flux closure and the capability to predict surface heat fluxes.

Update:

For this initial study a single mesh was used and buoyancy was neglected. The mesh contains approximately three million elements and four element topologies. The Reynolds number based on inlet velocity and rod diameter was $Re_D = 218,025$, inlet velocity $U_{in} = 5.0\ m/s$, Prandtl number $Pr = 1$, turbulent Prandtl number $Prt = 0.9$, inlet temperature $T_{in} = 150\ K$, $\dot{q}''_{w,bc} = 1.0E6\ W/m^2$, and $T_{w,bc} = 300\ K$, density $\rho = 918\ kg/m^3$, viscosity $\mu = 2.0E-4\ kg/ms$, specific heat $C_p = 4320\ J/kgK$ and conductivity $\kappa = 0.864\ W/mK$. Two cases; constant rod temperature and constant rod heat flux were investigated using SA and STD models.

The main objective in this study was to determine how accurately wall heat flux can be computed by Hydra-TH for the SA model using wall damping and $k-\varepsilon$ using wall functions. Since no validation data is available for this problem the quantity of interest was chosen to be energy balance. Energy balance is an integrated quantity that depends on the amount of heat entering the domain, flux introduced into the flow, and heat leaving and therefore, on how well the surface heat flux is computed. A simple energy balance is based on enthalpy

$$H = \int_c \rho C_p T \mathbf{u} \cdot \mathbf{n} dA_c$$

where T and $\mathbf{u} \cdot \mathbf{n}$ are integrated on inlet and outlet flow channel surfaces dA_c. The energy added to the system is due to conduction,

$$Q = \int_w \dot{q}''_w dA_w$$

where dA_w represents the differential wall area. The steady enthalpy balance is

$$H_{out} = H_{in} + Q.$$

Two estimates of heat flux for this problem are; finite-difference using the temperature modified by the actual heat flux (Equation 7) and the molecular thermal conductivity coefficient, and the wall function formulations, Equation 4 or Equation 5. In the case of constant heat flux wall boundary conditions, the wall temperature is inferred from the heat flux value, κ_{eff} and T_p using Equation 7. For the case of constant wall temperature boundary conditions, the wall function is used by the output delegate to compute the heat flux, Equation 4.

Total kinetic energy history is shown in Figure 23. Despite the violent swirl induced by mixing vanes, a relatively constant value is achieved for both SA and STD models. Helicity, a measure of swirling flow structure and temperature on the surface of the center rod for the STD model are shown in Figure 24. Swirl persists many rod diameters downstream enhancing mixing and heat transfer from the rod surface. Figure 25 shows the temperature of the center rod for the constant wall heat flux boundary condition case along with 14 transverse planes of the sub-channel fluid regions. Temperature increases along the span due to conduction from the rod surfaces.

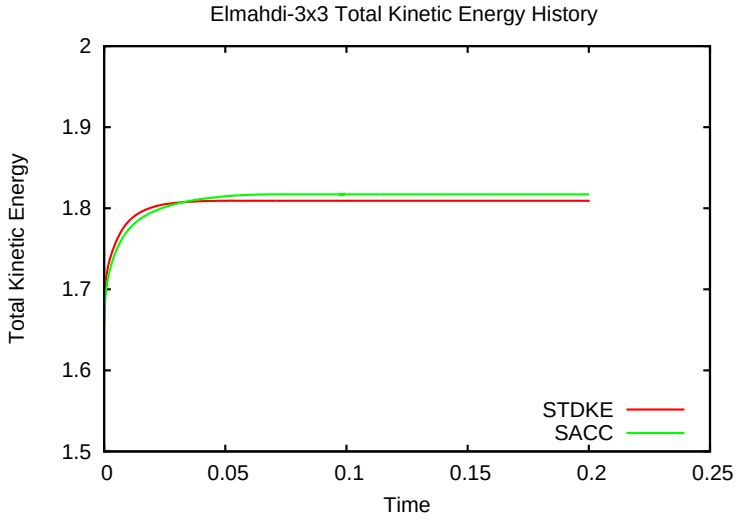

Figure 23: Elmahdi 3x3 rod/spacer grid. Total kinetic energy history.

Table 5 summarizes the energy balance for SA and STD models and different methods of computing wall heat flux. The y^+ and y^* values become quite large making the wall heat flux calculations very challenging. For conservative discretizations such as Hydra-TH, percent difference in energy balance is expected to be very close to zero. Deviation from zero is a measure of the error in wall heat flux calculation. In the first two rows of Table 5

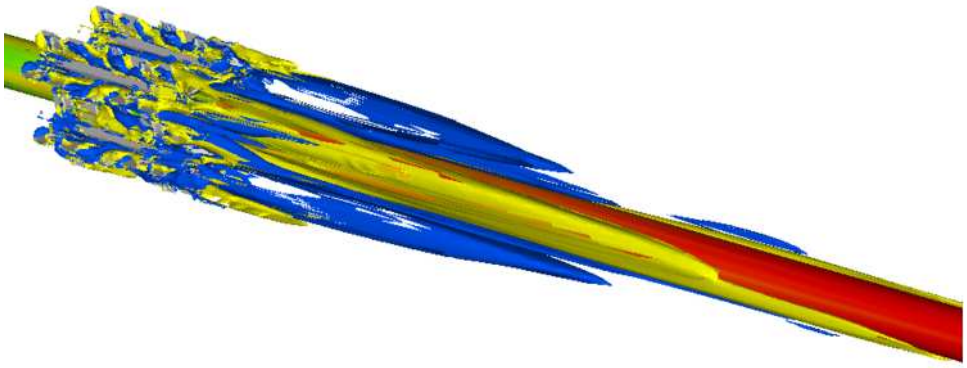

Figure 24: Elmahdi 3x3 rod/spacer grid. Temperature shown on center rod, helicity; positive is yellow, negative is blue.

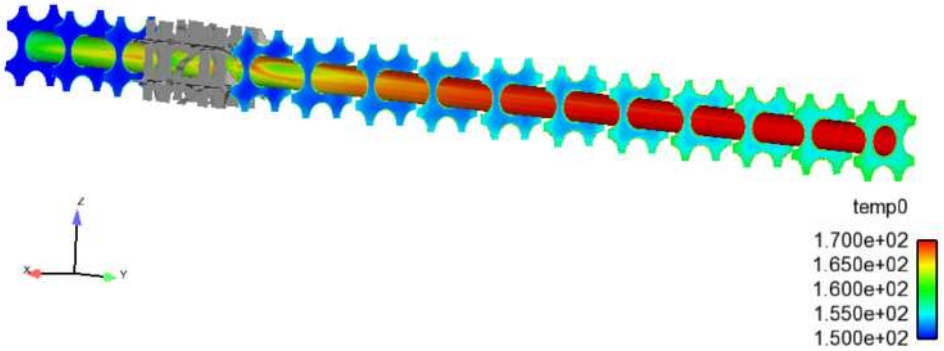

Figure 25: Elmahdi 3x3 rod/spacer grid. Temperature shown on center rod, y-planes show sub-channel fluid regions progressively heating up.

a constant heat flux boundary condition was specified, and in the last four rows, a constant wall temperature was specified.

For the case of constant wall heat flux boundary condition, a reasonable choice for the wall heat flux is the specified boundary condition value. However, due to the coarse mesh, the actual flux transported into the fluid is somewhat different. A similar situation occurred in the calculation of the Nusselt number in fully developed pipe flow § 9.7. This particular aspect of the output delegate in Hydra-TH is not fully understood at this time and should be investigated further.

For the case of constant wall temperature, the finite-difference estimate for wall heat flux using the molecular conductivity coefficient produces and unacceptably large error. When the Hydra-TH output delegate is used to represent wall heat flux the error is reduced by a factor of ten. It uses the effective wall function transport coefficient Equation 4. Interestingly, the finite-difference method used on the SA solution is more accurate than the output delegate. The Hydra-TH output delegate for SA does not use an effective transport coefficient so is not clear why this produces a greater error.

In summary, if the wall heat flux is specified, it should be used, otherwise for a specified temperature, and $k-\varepsilon$ model, the wall function should be used. In all cases the SA model that applies damping functions as opposed to wall functions is slightly more accurate.

Model	y^* (ave.) y^+ (ave.)	Wall BC	Hydra-TH delegate	$\dot{q}''_w$ f.d.	H_{in}	Total	H_{out}	% diff.
STD	18-2206(252)	const. $\dot{q}''_w$	NA	1,655 (mod.T)	1,019,647	1,021,302	1,038,597	1.7
SA	1-66(44)	const. $\dot{q}''_w$	NA	23,769 (mod.T)	1,056,631	1,080,400	1,084,112	0.3
STD	18-2206(252)	const. T_w	NA	13,715	1,042,958	1,056,674	1,395,642	24
STD	18-2206(252)	const. T_w	317,194	NA	1,042,958	1,360,152	1,395,642	2.5
SA	1-66(44)	const. T_w	NA	18,919	1,042,958	1,061,877	1,051,051	1.0
SA	1-66(44)	const. T_w	28,308	NA	1,042,958	1,071,266	1,051,051	2.0

Table 5: Elmahdi 3x3 rod/spacer grid sub-channel flow with heat transfer. STD $k-\varepsilon$ and SA turbulence models.

9.19 T-Junction Pipe Flow

Objectives:

1. Comparison of turbulence models on a CASL relevant flow problem.
2. Comparison of mean velocity and temperature profiles.

Resources:

1. Some work has been done (M.A. Christon), see the Hydra-TH V&V manual [10].
2. "Report of the OECD/NEA-Vattenfall T-Junction Benchmark Exercise," NEA/CSNI/R, May 2011. This report includes OECD/NEA-Vattenfall T-Junction Benchmark Specifications (Final Version, July 2009).
3. S. Jayaraju, E. Komen, and E. Baglietto, "Validation of STAR-CCM+ with the OECD/NEA T-Junction Blind Benchmark," presented at the STAR European Conference, March 22-23, 2011.
4. J-M Ndombo and R. Howard, "Large Eddy Simulation and the effect of the turbulent inlet conditions in the mixing Tee," Nuclear Engineering and Design, 241, pp. 2172-2183, 2011.

Tasks:

1. Define problem, gather references.
2. Build or obtain meshes.
3. Run the simulations with the different models.
4. Document results.
5. May require LES.
6. Compare RANS to LES solutions.

Comments and Status:

Pannala and Stagg [27] have simulated this flow using Star-CCM+ [6].

10 Summary and Recommendations

This document outlines a multi-year plan for developing enhanced turbulence modeling capabilities in Hydra-TH and updates the plan to include work accomplished this year. This is an extension of THM CASL milestone L3:THM.CFD.P10.02 [33] and picks up where it left off.

The development plan is organized into six sections and is scheduled to span two to three years. The six sections are:

1. Mature existing and implement new single-phase turbulence models in Hydra-TH.
2. Plan for and refactor/enhance near wall modeling to include both wall functions and low Re damping functions.
3. Plan for an extend models to treat buoyancy driven flows, both thermal and solutal.
4. Stretch goals: periodic and symmetry boundary conditions.
5. Miscellaneous items: limiting ε, inlet profiles and post-processing applications.
6. Define and construct and execute turbulence torture tests to assess capabilities and identify weaknesses.

In this first year maturation of the standard $k-\varepsilon$ and nonlinear $k-\varepsilon$ has taken place. This was largely accomplished using the turbulence torture test suite of problems. Also in the first year, the realizable $k\varepsilon$ model has been implemented and tested. All three models are now ready to be promoted to the master branch of the code base. The code resides in two branches of the LANL git repository; BenKE and tmsmithRKE. The second branch is a local branch and has not been pushed to the LANL repository.

A description of the current status of wall functions in Hydra-TH, damping function formulations and outline of a development plan to improve capabilities in this crucial area of turbulence modeling can be found in § 4. Several torture tests were designed to assess the wall function capability, specifically, Fully Developed Pipe Flow, Impinging Jet Flow and Elmahdi 3x3 Rod/Spacer Grid Flow, and make comparisons between the SA model using damping functions and the $k-\varepsilon$ models using the y*-insensitive wall function. The results show that the SA solutions for surface quantities are very accurate for the class of problems tested and that care must be exercised when extracting surface data from the $k-\varepsilon$ model solutions but if interpreted correctly are also accurate.

The Square Cavity problem was designed to exercise buoyancy terms in the momentum and turbulence model equations. The solution results are compared with experiments and agree favorably. This establishes a good launching point for next year's development plan.

Turbulent dissipation limiting currently used in Hydra-TH, called out in § 8 has been documented to serve as a future reference.

Progress in post-processing includes:

1. implementation of local-to-global element and node map writers for Exodus to allow distributed plot files to be joined into a single Exodus file,
2. interrogation of element data by node, element (Hydra-TH stores transported DoFs on elements), or sideset,
3. addition of wedge6, Pyramid5 element topologies to extract surface quantities on heterogeneous meshes,
4. algorithm for calculating Nu from Hydra-TH solution data.

Also in the first year a collection of turbulence benchmark problems have been constructed. Tests that have been completed or where significant progress has been made include:

1. Couette Flow - nearly complete, lack of asymmetry is a concern,
2. Backward Facing Step - simulations run, analysis yet to be done,
3. Fully Developed Pipe Flow - extensive testing on several models for wall shear and Nu,
4. Mixing Layer - extensive testing, scale similarity achieved on all models,
5. Grid Turbulence - completed for all $k - \varepsilon$ models,
6. Impinging Jet Flow - extensive testing, models perform as expected,
7. Elmahdi 3x3 Rod/Spacer Grid - testing complete for several model including heat transfer,
8. Square Cavity - simulations completed using several models, baseline buoyancy closure working
9. U-channel - see Smith and Christon [32] L3:THM.FD.P9.06.

Work completed by others include:

1. Channel Flow - see V&V manual [10],
2. Sub-Channel Secondary Flow - see Magolan et al. [24],
3. Mixing Layer - Magolan (see § 9.5).
4. Grid Turbulence - RNG model, see V&V manual [10],

Each section of the report contains sub-sections for; references/resources, tasks and status/comments, to be a resource for future work (see for example, § 3 - § 9). Sections that were worked on this year contain an additional update sub-section. Extensive reference lists accompany each sub-section.

In the second year the SST $k - \omega$ implementation is scheduled to begin. Also in the second year, near wall treatment for different variants of the $k - \varepsilon$ models and buoyancy

driven turbulence modeling is scheduled to begin. Near wall treatment work includes refactoring existing code and fundamental formulation work on low-Reynolds number damping functions and wall functions. The near wall treatment code will be refactored in order to encapsulate all modeling terms appearing in all of the governing equations to ensure consistency in the formulation, ease of implementation, to support new near wall treatments such as low-Re damping functions and consistency in surface delegate output quantities. Corrections/extensions, for buoyancy driven flows both thermal and solutal necessary for post LOCA accident scenarios where injection of highly borated coolant must be simulated, will be developed. Two-phase turbulence modeling is very important to the thermal hydraulics capability. However, this work is beyond the scope of the work described in this report which currently deals only with single-phase flows.

Recommendations based on this year's work are the following:

1. The source of non-asymmetry observed in Couette flow solutions of the SA model and more pronounced in the $k-\varepsilon$ models should be determined and remedied.

2. The accuracy of the SA model prediction of wall shear and heat flux for attached flows and even Elmahdi 3x3 rod/spacer grid flow compared with wall function based $k-\varepsilon$ solutions warrants development of low-Re $k-\varepsilon$ models.

3. The nonlinear stress-strain extension to the SA model proposed by Spalart [34] would only require a modest effort to implement and may substantially improve accuracy for secondary flow problems (see § 9.17).

4. Consistency between wall function based $k-\varepsilon$ solution data and suface delegate output of wall shear and heat flux should be strongly enforced.

This document is a work in progress. It will be periodically updated as new modeling requirements are mandated and as participation from team members grows.

References

[1] S. Allmaras, F. Johnson, and P. Spalart, *Modifications and clarifications for the implementation of the spalart-allmaras turbulence model ICCFD7-1902*, in Seventh International Conference on Computational Fluid Dynamics (ICCFD7), Big Island, Hawaii, July 9-13, 2012.

[2] E. Baglietto, *Anisotropic turbulence modeling for accurate rod bundle simulations*, in International Conference on Nuclear Engineering (ICONE14), Miami, Florida, USA, July 17-20 2006.

[3] E. Baglietto, M. Christion, J. Bakosi, B. Magolan, A. Manera, V. Petrov, and T. Smith, *Single phase validation of Hydra-TH for fuel applications*, Tech. Rep. FY14.CASL.010,L2:THM.P9.01, CASL, August 2014.

[4] E. Baglietto and H. Ninokata, *Improved turbulence modeling for performance evaluation of novel fuel designs*, Nuclear Technology, 158 (2007), pp. 237–248.

[5] J. Blazek, *Computational Fluid Dynamics: Principles and Applications*, Elsevier Science LTD, Kidlington, Oxford, UK, 2001.

[6] CD-Adapco, *STAR CCM+*.

[7] M. Christon, J. Bakosi, N. Barnett, M. Francois, and R. Lowrie, *HYDRA-TH L2 milestone*, Tech. Rep. LA-UR-11-07034, Los Alamos National Laboratory, Los Alamos, New Mexico, December 2011.

[8] M. Christon, J. Bakosi, M. Francois, and R. Nourgaliev, *HYDRA-TH theory manual*, Tech. Rep. LA-UR-11-05387, Los Alamos National Laboratory, Los Alamos, New Mexico, September 2011.

[9] M. A. Christon, J. Bakosi, R. Lowrie, B. Nadiga, Y. Xia, H. Luo, and A. Stagg, *HYDRA-TH user's manual*, Tech. Rep. LA-UR-14-23473, Los Alamos National Laboratory, Los Alamos, New Mexico, September 2014.

[10] M. A. Christon, B. Nadiga, J. Bakosi, L. Pritchett-Sheats, X. Yidong, L. Hong, W. Chuanjin, and R. Nourgaliev, *HYDRA-TH verification, validation and thermal hydraulics benchmark problems*, Tech. Rep. LA-UR-14-23461, Los Alamos National Laboratory, Los Alamos, New Mexico, May 2014.

[11] D. Coles, *The law of the wake in the turbulent boundary layer*, Journal of Fluid Mechanics, 1 (1956), pp. 191–226.

[12] A. Craft, T.J. Gerasimov, H. Iacovides, and B. Launder, *Progress in the generalization of wall-function treatments*, International Journal of Heat and Fluid Flow, 23 (2002), pp. 148–160.

[13] T. Craft, S. Gant, A. Gerasimov, H. Iacovides, and B. Launder, *Development and application of wall-function treatments for turbulent forced and mixed convection flows*, Fluid Dynamics Research, 38 (2006), pp. 127–144.

[14] T. Craft, B. Launder, and K. Suga, *Development and application of a cubic eddy-viscosity model of turbulence*, International Journal of Heat and Fluid Flow, 17 (1996), pp. 108–115.

[15] J. Dacles-Mariani, D. Kwak, and G. Zilliac, *On numerical errors and turbulence modeling in tip vortex flow prediction*, International Journal for Numerical Methods in Fluids, 30 (1999), pp. 65–82.

[16] J. Dacles-Mariani, G. Zilliac, J. Chow, and P. Bradshaw, *Numerical/experimental study of a wingtip vortex in the near field*, AIAA Journal, 33 (1995), pp. 1561–1568.

[17] L. Davidson, *Second-order corrections of the k-ϵ model to account for non-isotropic effects due to buoyancy*, International Journal for Heat and Mass Transfer, 133 (1990), pp. 2599–2608.

[18] H. Grotjans and F. Menter, *Wall functions for general application cfd codes*, ECCOMAS Proceedings of 4th European CFD Conference, (1998), pp. 1112–1117.

[19] K. Hanjalic and B. Launder, *Modelling Turbulence in Engineering, Second-Moment Routes to Closure*, Cambridge University Press, 2011.

[20] W. P. Jones and B. E. Launder, *The prediction of laminarization with with a two-equation model of turbulence*, International Journal of Heat and Mass Transfer, 15 (1972), pp. 301–314.

[21] ——, *The calculation of low-reynolds-number phenomena with a two-equation model of turbulence*, International Journal of Heat and Mass Transfer, 16 (1973), pp. 1119–1130.

[22] W. Kays and M. Crawford, *Convective Heat and Mass Transfer, 3rd Ed.*, McGraw-Hill Book Company, 1993.

[23] B. E. Launder and D. Spalding, *The numerical computation of turbulent flows*, Computer Methods in Applied Mechanics and Engineering, 3 (1974), pp. 269–289.

[24] B. Magolan, E. Baglietto, M. Christon, and T. Smith, *Non-linear eddy viscosity turbulence modeling in hydra-th for fuel related applications*, in The 16th International Topical Meeting on Nuclear Reactor Thermal Hydraulics (NURETH-16-13336), Hyatt Regency, Chicago, Il, August 30 - September 4 2015.

[25] F. Menter, *Two-equation eddy-viscosity turbulence models for engineering applications*, AIAA Journal, 32 (1994), pp. 1598–1605.

[26] D. Monson, H. Seegmiller, P. McConnaughey, and Y. Chen, *Comparison of experiment with calculations using curvature-corrected zero and two equation turbulence models for two-dimensional u-duct*, AIAA Paper 90-1484, (1990).

[27] S. Pannala and A. Stagg, *CFD THM: CFD benchmarks and test cases*, Technical Report, Oak Ridge National Laboratory, (2012).

[28] V. C. Patel, W. Rodi, and G. Scheuerer, *Turbulence Models for Near-Wall and Low Reynolds Number Flows: A Review*, AIAA Journal, 23 (1985), pp. 1308–1319.

[29] B. Petukhov, *Advances in Heat Transfer, vol. 6*, Academic Press, New York, 1970.

[30] T.-H. Shih, W. Liou, A. Shabbir, Z. Yang, and J. Zhu, *A new $k-\varepsilon$ eddy viscosity model for high reynolds number turbulent flows*, Computers and Fluids, 24 (1995), pp. 227–238.

[31] M. L. Shur, M. Strelets, A. K. Travin, and P. R. Spalart, *Turbulence modeling in rotating and curved channels: Assessing the spalart-shur correction*, AIAA Journal, 38 (2000), pp. 784–792.

[32] T. Smith and M. Christon, *Enhanced turbulence model capabilities in Hydra-TH*, Tech. Rep. L3:THM.CFD.P9.06, CASL, September 2014.

[33] T. Smith, M. Christon, M. Berndt, E. Baglietto, B. Magolan, A. Stagg, and H. Luo, *A multi-year plan for enhancing turbulence modeling in hydra-th*, Tech. Rep. L3:THM.CFD.P10.02, CASL, March, 31 2015.

[34] P. R. Spalart, *Strategies for turbulence modelling and simulations*, International Journal of Heat and Fluid Flow, (2000), pp. 252–263.

[35] P. R. Spalart and S. R. Allmaras, *A one-equation turbulence model for aerodynamic flows*, AIAA Paper 92-0439, (1992).

[36] P. R. Spalart, A. Garbaruk, and M. Strelets, *Rans solutions in couette flow with streamwise vorticity*, International Journal of Heat and Fluid Flow, (2014), pp. 128–134.

[37] P. R. Spalart and M. Shur, *On the sensitization of turbulence models to rotation and curvature*, Aerospace Science and Technology, (1997), pp. 297–302.

[38] D. C. Wilcox, *Reassessment of the Scale-Determining Equation for Advanced Turbulence Models*, AIAA Journal, 26 (1988), pp. 1299–1310.

[39] ——, *Turbulence Modeling for CFD*, DCW Industries Inc., 1998.

[40] V. Yakhot, S. Orszag, S. Thangam, T. Gatski, and G. Speziale, *Development of turbulence models for shear flows by a double expansion technique*, Physics of Fluids A: Fluid Dynamics, 4 (1992), pp. 1510–1520.

11 Appendix: Hydra-TH RANS Turbulence Models

This section is intended to provide a launching point for Reynolds averaged Navier-Stokes based turbulence modeling. A richer discussion can be found in the Hydra-TH theory manual [8]. It should serve as a reference for current capabilities, future development and special topics that need to be addressed. It also helps enforce consistent nomenclature between models which is valuable during the implementation phase of development.

To develop Reynolds averaged Navier-Stokes equations, a time averaging filter is applied to the dependent variables

$$\overline{u(x_i,t)} = \frac{1}{\Delta T}\int_t^{t+\Delta T} u(x_i,\mathcal{T})d\mathcal{T}.$$

With this definition, the instantaneous "exact" value can be decomposed into a mean and fluctuating component

$$u = \overline{u} + u'.$$

For the situation where density varies, the time average is mass weighted and a Favre average is defined

$$\widetilde{u(x_i,t)} = \frac{1}{\overline{\rho}\Delta T}\int_t^{t+\Delta T} \rho(x_i,\mathcal{T})u(x_i,\mathcal{T})d\mathcal{T}.$$

Similar to the time average, the instantaneous values and their relationship to the time averaged values are

$$u = \widetilde{u} + u'' \quad \widetilde{u} = \frac{\overline{\rho u}}{\overline{\rho}}.$$

And we note that these definitions imply the following

$$\overline{u'} = 0, \quad \overline{\overline{u}} = \overline{u}, \quad \widetilde{u''} = 0, \quad \widetilde{\widetilde{u}} = \widetilde{u}.$$

Strictly speaking, the averaging operation removes temporal dependence from the dependent variables, but in practice, this dependence is retained for convenience of solution and for hybrid unsteady RANS (URANS) modeling.

To start the discussion, the RANS equations for continuity, momentum and energy are shown to highlight the closure terms that must be modeled. These terms center around evaluation of eddy viscosity. The conservation of mass is written,

$$\frac{\partial\overline{\rho}}{\partial t} + \frac{\partial(\overline{\rho}\widetilde{v}_i)}{\partial x_i} = 0 \tag{24}$$

where the overbar $(\bar{\cdot})$ represents time average and the tilde $(\tilde{\cdot})$ represents mass weighted time average or Favre averaging. In this equation $\overline{\rho}$ is the density. The conservation of momentum is

$$\frac{\partial(\overline{\rho}\widetilde{v}_i)}{\partial t} + \frac{\partial(\overline{\rho}\widetilde{v}_i\widetilde{v}_j)}{\partial x_j} = -\frac{\partial\overline{p}}{\partial x_i} + \frac{\partial}{\partial x_j}\left[2\mu\widetilde{S}_{ij} - \frac{2}{3}\frac{\partial\widetilde{v}_k}{\partial x_k}\delta_{ij}\right] + \frac{\partial}{\partial x_j}(-\overline{\rho}\widetilde{v_i''v_j''}) - (\overline{\rho}-\rho_0)g_i \tag{25}$$

where $\widetilde{v}_i$ is the velocity vector, $\overline{p}$ is pressure, ρ_0 is a reference density, $\widetilde{S}_{ij}$ is the symmetric strain rate tensor

$$\widetilde{S}_{ij} = \frac{1}{2}\left(\frac{\partial\widetilde{v}_i}{\partial x_j} + \frac{\partial\widetilde{v}_j}{\partial x_i}\right) \tag{26}$$

μ is the dynamic viscosity, $-\overline{\rho}\widetilde{v_i''v_j''}$ are the Reynolds stresses that appear when the average operation is applied to the nonlinear advection term and $(v_i''(x_i,t))$ are the fluctuating velocity components in the Reynolds decomposition. A model is required to represent these stresses in order to close the momentum equations. The conservation of energy written for temperature is

$$\frac{\partial(\overline{\rho}C_p\widetilde{T})}{\partial t}+\frac{\partial(\overline{\rho}C_p\widetilde{v}_i\widetilde{T})}{\partial x_i}=-\frac{\partial\overline{q}_i}{\partial x_i}-\frac{\partial(\overline{\rho}\widetilde{h''v_i''})}{\partial x_i}+\dot{q} \tag{27}$$

where C_p is the specific heat at constant pressure and $\overline{q}_i$ is the heat flux vector assuming Fourier's law

$$\overline{q}_i=-\kappa\frac{\partial\widetilde{T}}{\partial x_i} \tag{28}$$

κ is the molecular thermal conductivity and $\dot{q}$ is a volumetric source such as radiation and $\overline{\rho}\widetilde{h''v_i''}$ is the turbulent heat flux.

The Reynolds stresses are modeled by the Boussinesq relationship

$$-\overline{\rho}\widetilde{v_i''v_j''}\approx\mu_t\left(2\widetilde{S}_{ij}-\frac{2}{3}\frac{\partial\widetilde{v}_k}{\partial x_k}\delta_{ij}\right)-\frac{2}{3}\overline{\rho}\delta_{ij}k \tag{29}$$

where μ_t is the eddy viscosity that must be determined and $k=\frac{1}{2}(\widetilde{v_k''v_k''})$ is the turbulent kinetic energy. The turbulent heat flux is modeled in a similar way dependent on the eddy viscosity and a turbulent Prandtl number (Pr_t)

$$\overline{\rho}\widetilde{h''v_i''}\approx\frac{C_p\mu_t}{Pr_t}\frac{\partial\widetilde{T}}{\partial x_i}=\kappa_t\frac{\partial\widetilde{T}}{\partial x_i}.$$

It is customary to lump the kinetic energy into the pressure

$$\hat{p}=\overline{p}+\frac{2}{3}\overline{\rho}k. \tag{30}$$

For incompressible flow, an additional Boussinesq relation is typically assumed for the body force

$$-(\overline{\rho}-\rho_0)g_i\approx-\rho_0\beta(\widetilde{T}-T_0)g_i \tag{31}$$

where $\beta=-\frac{1}{\rho}(\frac{\partial\rho}{\partial T})_p$ is a thermal expansion coefficient with units $(1/K)$, g_i is the gravity vector with units (m/s^2) and T_0 is a reference temperature and the divergence is zero. The RANS equations can be written in this simpler form

$$\begin{aligned}
\frac{\partial\overline{\rho}}{\partial t}+\frac{\partial(\overline{\rho}\widetilde{v}_i)}{\partial x_i} &= 0\\
\frac{\partial(\overline{\rho}\widetilde{v}_i)}{\partial t}+\frac{\partial(\overline{\rho}\widetilde{v}_i\widetilde{v}_j)}{\partial x_j} &= -\frac{\partial\hat{p}}{\partial x_i}+\frac{\partial}{\partial x_j}\left[2(\mu+\mu_t)\widetilde{S}_{ij}\right]-\beta(\widetilde{T}-T_0)g_i\\
\frac{\partial(\overline{\rho}C_p\widetilde{T})}{\partial t}+\frac{\partial(\overline{\rho}C_p\widetilde{v}_i\widetilde{T})}{\partial x_i} &= -\frac{\partial}{\partial x_i}\left[(\kappa+\kappa_t)\frac{\partial\widetilde{T}}{\partial x_i}\right]+\dot{q}
\end{aligned} \tag{32}$$

11.1 Spalart-Allmaras

The Spalart-Allmaras eddy viscosity transport model (SA) [35] is;

$$\frac{\partial \overline{\rho}\widetilde{\nu}}{\partial t} + \frac{\partial}{\partial x_j}\left(\overline{\rho}\widetilde{v}_j\widetilde{\nu}\right) = \overline{\rho}c_{b1}\widetilde{S}_a\widetilde{\nu} - \overline{\rho}c_{w1}f_w\left(\frac{\widetilde{\nu}}{d}\right)^2 + \frac{\partial}{\partial x_j}\left(\frac{\overline{\rho}}{\sigma}(\nu+\widetilde{\nu})\frac{\partial\widetilde{\nu}}{\partial x_j}\right) + \frac{\overline{\rho}c_{b2}}{\sigma}\frac{\partial\widetilde{\nu}}{\partial x_j}\frac{\partial\widetilde{\nu}}{\partial x_j}. \quad (33)$$

The eddy viscosity is given by,

$$\nu_t = \widetilde{\nu}f_{v1}. \quad (34)$$

Functions defining the damping function, source terms and non-conservative diffusion terms in the model are listed below;

$$f_w = g\left(\frac{1+C_{w3}^6}{g^6+C_{w3}^6}\right)^{1/6}, f_{v1} = \frac{\chi^3}{\chi^3+C_{v1}^3}, \quad f_{v2} = 1 - \frac{\chi}{1+\chi f_{v1}}, \quad (35)$$

$$\chi = \frac{\widetilde{\nu}}{\nu}, \quad g = r + C_{w2}(r^6 - r), \quad r = \frac{\widetilde{\nu}}{\widetilde{S}_a k^2 d^2}, \quad (36)$$

$$\widetilde{S}_a = S_r + \frac{\widetilde{\nu}f_{v2}}{k^2d^2}, \quad S_r = \sqrt{2\widetilde{R}_{ij}\widetilde{R}_{ij}}, \quad \widetilde{R}_{ij} = \frac{1}{2}\left(\frac{\partial\widetilde{v}_i}{\partial x_j} - \frac{\partial\widetilde{v}_j}{\partial x_i}\right), \quad (37)$$

where $\widetilde{R}_{ij}$ is the rotation tensor. Model parameters are listed in Table 6.

k	C_{b1}	C_{b2}	σ	C_{w1}	C_{w2}	C_{w3}	C_{v1}	C_{v2}
0.41	0.1355	0.622	2/3	$\frac{C_{b1}}{k^2} + \frac{1+C_{b2}}{\sigma}$	0.3	2.0	7.1	5.0

Table 6: Model parameters for Spalart-Allmaras turbulence model.

A different formula for $\widetilde{S}_a$ has been proposed in Blazek [5] (also used in Hydra-TH [8]) that prevents it from taking a value of zero. The modified $\widetilde{S}_a$ is;

$$\begin{aligned}
\widetilde{S}_a &= \widetilde{f}_{v3}S_r + \frac{\widetilde{\nu}f_{v2}}{k^2d^2}, \\
\widetilde{f}_{v2} &= \left(1 + \frac{\chi}{C_{v2}}\right)^{-3} \\
\widetilde{f}_{v3} &= \frac{(1+\chi f_{v1})(1-\widetilde{f}_{v2})}{\chi}.
\end{aligned} \quad (38)$$

k is von Karman's constant, and d appearing in the source terms represents the normal distance to the wall. At a solid wall, $\nu_t = 0$, and therefore the boundary condition is, $\widetilde{\nu}_w = 0$. At inflow boundaries $\widetilde{\nu}_{\Gamma_{Din}} \approx (3-5)\nu_\infty$ and and for outflow boundaries $\widetilde{\nu}_{\Gamma_{Nout}} = \frac{\partial\widetilde{\nu}}{\partial x_j}\hat{n}_j = 0$.

Eddy viscosity models that are used in RANS simulations such as the SA model typically contain a production source term that relates the production of eddy viscosity (in this case) to some measure of the mean shear. This is referred to as the Boussinesq approximation. The SA model makes use of the rotation tensor to estimate shear. In flows where significant vortical structure exists or geometric curvature, the eddy viscosity can be over predicted. There have been several "corrective measures" described in the literature to address this shortcoming in the model. The first correction is by Spalart and Shur [37], Shur et al. [31] (SA-S) and a second correction is due to Dacles-Mariani et al. [16] [15] (SA-DM).

The Shur et al. correction is very invasive requiring the computation of material derivatives for the symmetric stress tensor which practically amounts to solving six additional transport equations. The Dacles-Mariani et al. correction only requires a modification to the production term. The Shur et al. correction was considered to be out-side the scope of this exploratory milestone and so the Dacles-Mariani correction was pursued instead.

Examination of the production source term;

$$P(\widetilde{\nu}) = \overline{\rho} c_{b1} \widetilde{S}_a \widetilde{\nu} \tag{39}$$

shows a dependence on the magnitude of the mean rotation through $\widetilde{S}_a$ and on $\widetilde{\nu}$ itself. In flows with significant vortical structure or geometric curvature, this can lead to an over-prediction in the eddy viscosity. Dacles-Mariani et al. [16] proposed a modification to the production term that accounts for solid-body-rotation and curvature by distinguishing between mean shear and mean rotation;

$$P(\widetilde{\nu}) = \overline{\rho} c_{b1} \widetilde{\nu} \left[(S_r + 2\min(0, \quad S_s - S_r)) + \frac{\widetilde{\nu} f_{v2}}{k^2 d^2} \right]. \tag{40}$$

In this equation, S_s is the magnitude of the symmetric stress tensor;

$$S_s = \sqrt{2 \widetilde{S}_{ij} \widetilde{S}_{ij}}, \qquad \widetilde{S}_{ij} = \frac{1}{2} \left(\frac{\partial \widetilde{v}_{ij}}{\partial x_j} + \frac{\partial \widetilde{v}_{ij}}{\partial x_j} \right). \tag{41}$$

Recently, professor Hong Luo at North Carolina State University brought to our attention modifications to the Spalart-Allmaras model [1] that are receiving a lot of attention in the aerospace community. An evaluation as to whether these modifications should be incorporated into Hydra-TH will be made.

A relatively simple extension has been added to the original model by Spalart [34, 36] the enables the model to capture secondary flows. The extension is similar to the extension added to the standard $k-\varepsilon$ model to create the nonlinear $k-\varepsilon$. In nonlinear eddy viscosity models, the constitutive relation between Reynolds stress and mean strain rate is nonlinear instead of the traditional linear model $-\overline{v_i'' v_j''} = \overline{\tau_{ij}} = 2\nu_t \overline{S}_{ij}$. Here, the overline denotes time averaging instead of Favre averaging. The nonlinear extension is

$$\tau_{ij} = \overline{\tau_{ij}} - c_{cr1}[O_{ik}\overline{\tau_{jk}} - O_{jk}\overline{\tau_{ik}}]$$

where

$$O_{ik} = \frac{\left(\frac{\partial \widetilde{v}_i}{\partial x_k} - \frac{\partial \widetilde{v}_k}{\partial x_i} \right)}{\sqrt{\partial \widetilde{v}_m / \partial x_n \partial \widetilde{v}_m / \partial x_n}}$$

is the normalized rotation tensor and $c_{cr1} = 0.3$ is a constant.

11.2 Standard $k-\varepsilon$ Model

See Hydra-TH theory manual [8] for a detailed discussion of the standard model. The model closure for the Reynolds stresses is reproduced from the above discussion (Equation 29)

$$-\overline{\rho}\widetilde{v_i''v_j''} \approx \mu_t\left(2\widetilde{S}_{ij} - \frac{2}{3}\frac{\partial\widetilde{v}_k}{\partial x_k}\delta_{ij}\right) - \frac{2}{3}\overline{\rho}\delta_{ij}k. \tag{42}$$

The "standard" $k-\varepsilon$ model of Jones and Launder [20] [21] for high-Reynolds number, including buoyancy effects is written

$$\begin{aligned}
\frac{\partial\overline{\rho}k}{\partial t} + \frac{\partial}{\partial x_j}\left(\overline{\rho}\widetilde{v}_j k\right) &= \frac{\partial}{\partial x_j}\left((\overline{\mu}+\mu_t/\sigma_k)\frac{\partial k}{\partial x_j}\right) + P_k + G_B - \overline{\rho}\varepsilon \\
\frac{\partial\overline{\rho}\varepsilon}{\partial t} + \frac{\partial}{\partial x_j}\left(\overline{\rho}\widetilde{v}_j \varepsilon\right) &= \frac{\partial}{\partial x_j}\left((\overline{\mu}+\mu_t/\sigma_\varepsilon)\frac{\partial \varepsilon}{\partial x_j}\right) + C_{\varepsilon 1}\frac{\varepsilon}{k}P_k + C_{\varepsilon 1}\frac{\varepsilon}{k}G_B - C_{\varepsilon 2}\overline{\rho}\frac{\varepsilon^2}{k}
\end{aligned} \tag{43}$$

where the production is defined as;

$$P_k = -\overline{\rho}\widetilde{v_i''v_j''}\frac{\partial\widetilde{v}_i}{\partial x_j}$$

and the eddy viscosity is define as;

$$\mu_t = \frac{C_\mu\overline{\rho}k^2}{\varepsilon}.$$

Production due to buoyancy has been modeled as (Davidson [17]),

$$G_B = -\frac{\mu_t}{\sigma_T}\beta_T g_i\frac{\partial\widetilde{T}}{\partial x_i}.$$

The model constants $C_{\varepsilon 1}$, $C_{\varepsilon 2}$, C_μ, σ_k, σ_ε and σ_T are presented in Table 7.

$C_{\varepsilon 1}$	$C_{\varepsilon 2}$	C_μ	σ_k	σ_ε	σ_T
1.44	1.92	0.09	1.0	1.3	0.85

Table 7: Model parameters for Standard $k-\varepsilon$ turbulence model.

11.3 RNG $k-\varepsilon$ Model

The Renormalization Group Theory (RNG) model was developed by Yakhot et al. [40]. See Hydra-TH theory manual [8] for a detailed discussion of the RNG model. The model equations for k and ε are the same as the standard model equations. RNG and standard models differ by the choice of model coefficients. The model closure for the Reynolds stresses is reproduced from the above discussion (Equation 29)

$$-\overline{\rho}\widetilde{v_i''v_j''} \approx \mu_t\left(2\widetilde{S}_{ij} - \frac{2}{3}\frac{\partial\widetilde{v}_k}{\partial x_k}\delta_{ij}\right) - \frac{2}{3}\overline{\rho}\delta_{ij}k. \tag{44}$$

The model equations for high-Reynolds number are

$$\begin{aligned}\frac{\partial \overline{\rho} k}{\partial t}+\frac{\partial}{\partial x_j}\left(\overline{\rho}\widetilde{v}_j k\right) &= \frac{\partial}{\partial x_j}\left((\overline{\mu}+\mu_t/\sigma_k)\frac{\partial k}{\partial x_j}\right)+P_k-\overline{\rho}\varepsilon \\ \frac{\partial \overline{\rho} \varepsilon}{\partial t}+\frac{\partial}{\partial x_j}\left(\overline{\rho}\widetilde{v}_j \varepsilon\right) &= \frac{\partial}{\partial x_j}\left((\overline{\mu}+\mu_t/\sigma_\varepsilon)\frac{\partial \varepsilon}{\partial x_j}\right)+C_{\varepsilon 1}\frac{\varepsilon}{k}P_k-C_{\varepsilon 2}\overline{\rho}\frac{\varepsilon^2}{k}\end{aligned} \tag{45}$$

where the production is defined as;

$$P_k=-\overline{\rho}\widetilde{v_i''v_j''}\frac{\partial \widetilde{v}_i}{\partial x_j}$$

and the eddy viscosity is define as;

$$\mu_t=\frac{C_\mu \overline{\rho} k^2}{\varepsilon}.$$

One of the main operational differences between the standard and RNG models is the definition of $C_{\varepsilon 2}$ which is no longer a constant but now depends on the mean strain rate

$$C_{\varepsilon 2}=\widetilde{C}_{\varepsilon 2}+\frac{C_\mu \eta^3(1-\eta/\eta_0)}{1+\beta\eta^3},\quad \eta=\frac{k}{\varepsilon}\sqrt{2\widetilde{S}_{ij}\widetilde{S}_{ij}},\quad \widetilde{S}_{ij}=\frac{1}{2}\left(\frac{\partial \widetilde{v}_i}{\partial x_j}+\frac{\partial \widetilde{v}_j}{\partial x_i}\right). \tag{46}$$

The model constants $C_{\varepsilon 1}$, $\widetilde{C}_{\varepsilon 2}$, C_μ, σ_k, σ_ε β and η_0 are presented in Table 8.

$C_{\varepsilon 1}$	$\widetilde{C}_{\varepsilon 2}$	$C_{\varepsilon 2}$	C_μ	σ_k	σ_ε	β	η_0
1.42	1.68	Eq. 46	0.085	0.72	0.72	0.012	4.38

Table 8: Model parameters for RNG $k-\varepsilon$ turbulence model.

11.4 Nonlinear $k-\varepsilon$ Model Design and Implementation

This work was done in support of a level 2 milestone entitled "Single Phase Validation of Hydra-TH for Fuel Applications (FY14.CASL.010)" [3]. One objective was to design, implement and validate the nonlinear $k-\varepsilon$ model of Baglietto [2] and Baglietto and Ninkata [4] in Hydra-TH. Work remains to mature this model to point where it is production ready. A brief description of the model is included here to facilitate the task of documenting it at a later date in the Hydra-TH theory manual. The description follows closely Baglietto [2].

The "standard" $k-\varepsilon$ model of Jones and Launder [20] can be written as;

$$\begin{aligned}\frac{\partial \overline{\rho} k}{\partial t}+\frac{\partial}{\partial x_j}\left(\overline{\rho}\widetilde{v}_j k\right) &= \frac{\partial}{\partial x_j}\left((\overline{\mu}+\mu_t/\sigma_k)\frac{\partial k}{\partial x_j}\right)P_k-\overline{\rho}\varepsilon \\ \frac{\partial \overline{\rho} \varepsilon}{\partial t}+\frac{\partial}{\partial x_j}\left(\overline{\rho}\widetilde{v}_j \varepsilon\right) &= \frac{\partial}{\partial x_j}\left((\overline{\mu}+\mu_t/\sigma_\varepsilon)\frac{\partial \varepsilon}{\partial x_j}\right)+C_{\varepsilon 1}\frac{\varepsilon}{k}P_k-C_{\varepsilon 2}\overline{\rho}\frac{\varepsilon^2}{k}\end{aligned} \tag{47}$$

where the production is defined as;

$$P_k=-\overline{\rho}\widetilde{v_i''v_j''}\frac{\partial \widetilde{v}_i}{\partial x_j}$$

and the eddy viscosity is define as;

$$\mu_t = \frac{C_\mu \overline{\rho} k^2}{\varepsilon}.$$

Unlike the standard model C_μ is not constant. Based upon realizability considerations, C_μ is a function of the shear and rotation invariants S and W,

$$C_\mu = \frac{C_{a0}}{(C_{a1} + C_{a2} S + C_{a3} W)} \tag{48}$$

where,

$$S = \frac{k}{\varepsilon}\sqrt{2\widetilde{S}_{ij}\widetilde{S}_{ij}}, \quad W = \frac{k}{\varepsilon}\sqrt{2\widetilde{\Omega}_{ij}\widetilde{\Omega}_{ij}},$$

$$\widetilde{S}_{ij} = \left(\frac{\partial \widetilde{v}_i}{\partial x_j} + \frac{\partial \widetilde{v}_j}{\partial x_i}\right), \quad \widetilde{\Omega}_{ij} = \left(\frac{\partial \widetilde{v}_i}{\partial x_j} - \frac{\partial \widetilde{v}_j}{\partial x_i}\right).$$

The Reynolds's stresses are represented by a nonlinear stress-strain relationship, necessary to capture anisotropic stress behavior which is responsible for the creation of secondary flow in fuel rod bundle flows. The quadratic stress-strain relationship is given by;

$$\begin{aligned}
\overline{\rho}\widetilde{v_i'' v_j''} &= \left(\frac{2}{3}\overline{\rho} k \delta_{ij} - \mu_t \widetilde{S}_{ij}\right) \\
&+ C_1 \mu_t \frac{k}{\varepsilon}\left[\widetilde{S}_{ik}\widetilde{S}_{kj} - \frac{1}{3}\delta_{ij}\widetilde{S}_{kl}\widetilde{S}_{kl}\right] \\
&+ C_2 \mu_t \frac{k}{\varepsilon}\left[\widetilde{\Omega}_{ik}\widetilde{S}_{kj} + \widetilde{\Omega}_{jk}\widetilde{S}_{ki}\right] \\
&+ C_3 \mu_t \frac{k}{\varepsilon}\left[\widetilde{\Omega}_{ik}\widetilde{\Omega}_{jk} - \frac{1}{3}\delta_{ij}\widetilde{\Omega}_{kl}\widetilde{\Omega}_{kl}\right]
\end{aligned}$$

where the first term on the right-hand-side is the usual linear contribution. For realizability, the three constants, (C_1, C_2, C_3) are non-constant given by;

$$C_1 = \frac{C_{NL1}}{(C_{NL6} + C_{NL7} S^3) C_\mu} \quad C_2 = \frac{C_{NL2}}{(C_{NL6} + C_{NL7} S^3) C_\mu} \quad C_3 = \frac{C_{NL3}}{(C_{NL6} + C_{NL7} S^3) C_\mu}$$

Model parameters are listed in Table 9 and Table 10.

C_μ	σ_k	σ_ε	$C_{\varepsilon 1}$	$C_{\varepsilon 2}$	C_{a0}	C_{a1}	C_{a2}	C_{a3}
Eq. 48	1.0	1.22	1.44	1.92	0.667	3.9	1.0	0

Table 9: Model parameters for nonlinear $k - \varepsilon$ turbulence model.

C_{NL1}	C_{NL2}	C_{NL3}	C_{NL6}	C_{NL7}
0.8	11	4.5	1000	1.000

Table 10: Model parameters for nonlinear $k - \varepsilon$ turbulence model quadratic stress terms.

The current implementation uses the y*-insensitive wall function described in the Hydra-TH theory manual. Baglietto and Ninokata [4] present damping functions to allow integration to the wall. These functions have not been implemented yet. In addition, the current implementation neglects sensitivities of the nonlinear stress terms in the implicit left-hand-side operator and so currently, the Jacobian terms for the nonlinear model are identical to the standard model. This choice was expedient and will have to be re-evaluated at a later time.

11.5 Realizable $k-\varepsilon$ Model

The Boussinesq relationship relating Reynolds stresses to the mean strain rate

$$-\overline{\rho}\widetilde{v_i''v_j''} \approx \mu_t \left(2\widetilde{S}_{ij} - \frac{2}{3}\frac{\partial \widetilde{v}_k}{\partial x_k}\delta_{ij}\right) - \frac{2}{3}\overline{\rho}\delta_{ij}k \tag{49}$$

and eddy viscosity for $k-\varepsilon$ given by

$$\mu_t = \overline{\rho}C_\mu \frac{k^2}{\varepsilon} \tag{50}$$

where $C_\mu = 0.09$ is a constant, can result in negative normal Reynolds stresses for large mean strain $\widetilde{S}$

$$\widetilde{S} = \sqrt{2\widetilde{S}_{ij}\widetilde{S}_{ij}}, \quad \widetilde{S}_{ij} = \frac{1}{2}\left(\frac{\partial \widetilde{v}_i}{\partial x_j} + \frac{\partial \widetilde{v}_j}{\partial x_i}\right), \quad \widetilde{\Omega}_{ij} = \frac{1}{2}\left(\frac{\partial \widetilde{v}_i}{\partial x_j} - \frac{\partial \widetilde{v}_j}{\partial x_i}\right)$$

and violate the Schwartz inequality for Reynolds stresses

$$\begin{array}{rcl} \overline{(v'_\alpha v'_\alpha)} & \geq & 0 \\ \overline{(v'_\alpha v'_\beta)^2} & \leq & \overline{(v'_\alpha)^2 (v'_\beta)^2}. \end{array}$$

The model of Shih et al. [30] which will be referred to as Realizable $k-\varepsilon$ is written as

$$\begin{array}{rcl} \dfrac{\partial \overline{\rho}k}{\partial t} + \dfrac{\partial}{\partial x_j}\left(\overline{\rho}\widetilde{v}_j k\right) & = & \dfrac{\partial}{\partial x_j}\left((\overline{\mu} + \mu_t/\sigma_k)\dfrac{\partial k}{\partial x_j}\right) + P_k - \overline{\rho}\varepsilon \\ \dfrac{\partial \overline{\rho}\varepsilon}{\partial t} + \dfrac{\partial}{\partial x_j}\left(\overline{\rho}\widetilde{v}_j \varepsilon\right) & = & \dfrac{\partial}{\partial x_j}\left((\overline{\mu} + \mu_t/\sigma_\varepsilon)\dfrac{\partial \varepsilon}{\partial x_j}\right) + \overline{\rho}C_1\widetilde{S}\varepsilon - \overline{\rho}C_2\dfrac{\varepsilon^2}{k + \sqrt{\nu\varepsilon}} \end{array} \tag{51}$$

The model constant C_1 is

$$C_1 = \max\left[0.43, \frac{\eta}{\eta + 5}\right], \quad \eta = \widetilde{S}\frac{k}{\varepsilon} \tag{52}$$

and the production is defined as;

$$P_k = -\overline{\rho}\widetilde{v_i''v_j''}\frac{\partial \widetilde{v}_i}{\partial x_j}.$$

Shih et al. [30] proposed a remedy for this deficiency by making C_μ a function of the mean strain

$$C_\mu = \frac{1}{A_0 + A_s U^* \frac{k}{\varepsilon}} \tag{53}$$

and

$$U^* = \sqrt{\widetilde{S}_{ij}\widetilde{S}_{ij} + \widetilde{\Omega}'_{ij}\widetilde{\Omega}'_{ij}} \quad \widetilde{\Omega}'_{ij} = \widetilde{\Omega}_{ij} - 2\varepsilon_{ijk}\omega_k \quad \widetilde{\Omega}_{ij} = \overline{\Omega}_{ij} - \varepsilon_{ijk}\omega_k \tag{54}$$

where $\overline{\Omega}_{ij}$ is the mean rotation rate viewed in a rotating reference frame and ω_k is the angular velocity ($rad/sec.$). For a non-rotating reference frame, $\widetilde{\Omega}'_{ij} = \widetilde{\Omega}_{ij}$, the usual definition for the rotation tensor. (This aspect of the model is a little confusing and needs to be examined more carefully.) The model constant A_s is

$$A_s = \sqrt{6}\cos\phi$$

where

$$\phi = \frac{1}{3}\cos^{-1}(\sqrt{6}W), \quad W = \frac{\widetilde{S}_{ij}\widetilde{S}_{jk}\widetilde{S}_{ki}}{(\widetilde{S}_{ij}\widetilde{S}_{ij})^{3/2}}. \tag{55}$$

The model constants C_1, C_2, σ_k and σ_ε are listed in Table 11.

C_μ	C_1	C_2	σ_k	σ_ε	A_0
Eq. 53	Eq. 52	1.9	1.0	1.2	4.0

Table 11: Model parameters for Realizable $k-\varepsilon$ turbulence model.

11.6 SST $k-\omega$ Model

Menter's shear stress transport (SST) $k-\omega$ model [25] blends Wilcox's $k-\omega$ model [38] with the standard $k-\varepsilon$ model where the ε equation, representing the rate of turbulent kinetic energy dissipation, is rewritten as an equation for ω, which approximately represents the time scale for energy dissipation. Units for $\varepsilon \rightarrow (\ell^2/t^3)$ and for $\omega \rightarrow (1/t)$. Several motivations for choosing this model over the standard $k-\varepsilon$ or the $k-\omega$ model are; The $k-\omega$ model and SST version do not require the use of special near wall treatments and can be integrated to the wall directly, eliminates the sensitivity to free stream ω that hampers the Wilcox $k-\omega$ model and incorporates transport of Reynolds stress (as the name implies) which results in better predictions in flows with strong pressure gradients. See Hydra-TH theory manual [8] for a detailed discussion of the SST $k-\omega$ model. The model closure for the Reynolds stresses is reproduced from the above discussion (Equation 29)

$$-\overline{\rho}\widetilde{v''_i v''_j} \approx \mu_t\left(2\widetilde{S}_{ij} - \frac{2}{3}\frac{\partial \widetilde{v}_k}{\partial x_k}\delta_{ij}\right) - \frac{2}{3}\overline{\rho}\delta_{ij}k. \tag{56}$$

The model equations are

$$\begin{aligned}
\frac{\partial \overline{\rho}k}{\partial t} + \frac{\partial}{\partial x_j}(\overline{\rho}\widetilde{v}_j k) &= \frac{\partial}{\partial x_j}\left((\overline{\mu} + \mu_t/\sigma_k)\frac{\partial k}{\partial x_j}\right) + P_k - \overline{\rho}\beta^* k\omega \qquad (57)\\
\frac{\partial \overline{\rho}\omega}{\partial t} + \frac{\partial}{\partial x_j}(\overline{\rho}\widetilde{v}_j \omega) &= \frac{\partial}{\partial x_j}\left(\overline{\rho}(\overline{\nu} + \sigma_\omega \nu_t)\frac{\partial \omega}{\partial x_j}\right) - \frac{\gamma}{\nu_t}P_k - \overline{\rho}\beta\omega^2 + 2(1-F_1)\overline{\rho}\sigma_{\omega 2}\frac{1}{\omega}\frac{\partial k}{\partial x_j}\frac{\partial \omega}{\partial x_j}
\end{aligned}$$

where the production is defined as;

$$P_k = -\overline{\rho}\widetilde{v_i''v_j''}\frac{\partial \widetilde{v_i}}{\partial x_j}$$

and the eddy viscosity is define as

$$\nu_t = \frac{a_1 k}{\max(a_1\omega; \Omega F_2)}.$$

where $\Omega = |\nabla \times \widetilde{\mathbf{v}}|$ is taken as the absolute value of vorticity and $\mu_t = \overline{\rho}\nu_t$. The blending function is defined

$$F_1 = \tanh(arg_1^4), \quad arg_1 = \min\left(\max\left(\frac{\sqrt{k}}{0.09\omega y}; \frac{500\overline{\nu}}{\omega y^2}\right); \frac{4\overline{\rho}\sigma_{\omega 2}k}{CDy^2}\right)$$

$$CD = \max\left(2\overline{\rho}\sigma_{\omega 2}\frac{1}{\omega}\frac{\partial \omega}{\partial x_j}\frac{\partial k}{\partial x_j}; 10^{-20}\right)$$

$$F_2 = \tanh(arg_2^2), \quad arg_2 = \max\left(2\frac{\sqrt{k}}{0.09\omega y}; \frac{500\overline{\nu}}{\omega y^2}\right).$$

Constants for the inner region (set 1) and the outer region (set 2) are blended

$$g(\phi_1, \phi_2; F_1) = F_1\phi_1 + (1 - F_1)\phi_2. \tag{58}$$

Model constants for a_1, β^*, and κ along with blended constants σ_k, σ_ω, β and γ are presented in Table 12 and the inner and outer set constants are presented in Table 13.

σ_k	σ_ω	β	γ	a_1	β^*	κ
$g(\sigma_{k1}, \sigma_{k2})$	$g(\sigma_{\omega 1}, \sigma_{\omega 2})$	$g(\beta_1, \beta_2)$	$g(\gamma_1, \gamma_2)$	0.31	0.09	0.41

Table 12: Blended model parameters for SST $k - \omega$ turbulence model.

σ_{k1}	$\sigma_{\omega 1}$	β_1	γ_1
0.85	0.5	0.075	$\beta_1/\beta^* - \sigma_{\omega 1}\kappa^2/\sqrt{\beta^*}$
σ_{k2}	$\sigma_{\omega 2}$	β_2	γ_2
1.0	0.856	0.0828	$\beta_2/\beta^* - \sigma_{\omega 2}\kappa^2/\sqrt{\beta^*}$

Table 13: Inner (set 1) and outer (set 2) parameters for SST $k - \omega$ turbulence model.

The free stream boundary conditions for ω, ν_t and k are

$$\omega_{\Gamma_{Din}} = (1 \to 10)\frac{V_\infty}{L}, \quad \nu_{t\Gamma_{Din}} = 10^{-(2\to 5)}\nu_\infty, \quad k_{\Gamma_{Din}} = \nu_{t\infty}\omega_{\Gamma_{Din}}.$$

The wall boundary conditions for ω and k are

$$\omega_{\Gamma_{Dwall}} = 10\frac{6\nu}{\beta_1(\Delta y_1)^2}, \quad k_{\Gamma_{Dwall}} = 0$$

where Δy_1 is the distance to the next point away from the wall. This boundary condition simulates a smooth wall where $\Delta y_1^+ < 3$ is assumed.

DISTRIBUTION:

1	MS 2222	Vincent A. Mousseau, 1441
1	MS 1320	Russell Hooper, 1446
1	MS 1320	Thomas M. Smith, 1446
1	MS 1320	Randall M. Summers, 1446
1	MS 0899	Technical Library, 9536 (electronic copy)

Sandia National Laboratories